NASA-CR-196589

[redacted]

Modeling the Effect of Shroud Contact and Friction Dampers on the Mistuned Response of Turbopumps

Final Report

Contract No. NAS8-38348

George C. Marshall Space Flight Center
National Aeronautics and Space Administration
Marshall Space Flight Center, AL 35812

J. H. Griffin and M-T. Yang
Department of Mechanical Engineering
Carnegie Mellon University
Pittsburgh, PA 15213

January 1994

INTRODUCTION AND BACKGROUND

Originally the goal of this contract was to develop a method for analyzing the structural response of mistuned bladed disk with nonlinear constraints such as shroud contact and friction damping. The approach was to used harmonic balance methods of approximating nonlinear response, and efficient, receptance methods for representing the linear substructures. It was postulated that the receptance approach could be used to reduce the number of degrees of freedom to just those directly associated with the nonlinear constraints. The harmonic balance method of dealing with the nonlinearities would replace a system of nonlinear ordinary differential equations with a system of nonlinear algebraic equations. Thus, using both approaches the calculation of the response of a mistuned bladed disk, such as the NASA turbopump would be reduced to that of solving a relatively small system of nonlinear algebraic equations.

Several primary objectives had to be achieved in order to meet these objectives. They were:

1. The response of the system with nonlinearities had to be nearly harmonic and have unique solutions.

2. The receptance method had to be developed to a point where it accurately predicted system response, and, yet was computationally efficient.

Initial studies were done during the first two years of this contract addressing the first issue of representing nonlinearities. Two types of nonlinearities were studied: the impact of neighboring shrouds, and friction dampers. It was found that for the case of neighboring shrouds hitting each other that the problem could have multiple solutions, even in the case of one blade. This meant that it was not feasible to include this type of physics (shroud lift-off or shroud hitting) when trying to simulate the response of bladed disks since the large number of possible solutions that could occur with multiple blades would make this problem extremely difficult to solve. It was found in the initial study, that friction constraints, on the other hand, always resulted in unique solutions that could be represented very well using harmonic balance methods. Consequently, it was decided to go ahead with the second part of the project, but include only friction-type nonlinearities in our formulation.

A result of this original study was that it was shown that some very unusual dynamic response that had been observed in a NASA turbopump was very possibly due to shroud contact. This work is documented in [1].

A formulation was then developed for reducing the number of degrees of freedom in a mistuning analysis. Initial work had been done in developing this approach when NASA decided that it had to significantly reduce funding for this project. As a consequence, it was agreed that the statement of work for this contract would be revised and the deliverables changed to the following:

- Complete the development of a computer code for performing linear mistuning analyses with reduced order models developed from a SPAR/EAL finite element model of the blade and an annular disk. Reduced order models are models that can be explicitly derived from the finite element model and that have significantly fewer degrees of freedom than a comparable finite element model, e.g., 10,000 degrees of freedom per blade reduced to six.

- The code will be based on a Monte Carlo type analysis in which the frequencies of the blades vary randomly and the forced response is calculated over a range of excitation frequencies.

- Document linear mistuning code.

- Prepare a paper on the mistuning analysis of a NASA turbopump for the Advanced Earth-to-Orbit Propulsion Technology — 1994 Conference.

Consequently, the final effort on this contact has focused on developing a linear mistuning code and that development and documentation is the focus of this report. A paper on the mistuning analysis of a NASA turbopump is included in volume II of the Proceedings of the Advanced Earth-to-Orbit Propulsion Technology — 1994 Conference and is cited as reference 2.

DEVELOPMENT AND DOCUMENTATION OF LINEAR MISTUNING CODE

The development and documentation of the linear mistuning code is documented in the three appendices of this report. They are:

- Appendix A: Summary Report. This summary report provides a brief summary of the theory and application of the linear mistuning code.

- Appendix B: User Manual. This manual specifies the input requirements for running the linear mistuning code.

- Appendix C: Theoretical Manual. This manual provides a detailed explanation of the theory and application of the linear mistuning code (in effect, this is an expanded version of Appendix A).

DELIVERY OF LINEAR MISTUNING CODE

The linear mistuning computer code (LMCC) and the input files used in analyzing the NASA turbopump have been transferred to NASA Marshall Silicon Graphics Computer on which the researchers where given an account. The example case, the NASA turbopump, ran correctly on the NASA computer. There was a problem with compatibility in transferring to the Silicon Graphics computer at NASA in that the random number generating subroutine did not work correctly on the Silicon Graphics if certain optimization options were used during its compilation. This problem is documented in the User Manual.

Thus, LMCC and example files have been successfully delivered to NASA Marshall at this time.

KEY RESULTS

Interesting results from running LMCC are discussed at some length in Appendix A. Briefly, however there are two key results:

1. It works well, i.e., it is computationally efficient and accurate.

2. When the disk is stiff, it predicts very different mistuned response from the mass spring models that were used in the past. LMCC shows that bladed disk systems can have a large amount of amplitude scatter from blade to blade even when the disk is very stiff. The old mass/spring models predict that, in this case, the blades would act as uncoupled, independent systems (the disk is almost a rigid foundation) and that there would be very little amplitude scatter. This could be a very important result if NASA decides to go to bladed disk systems with stiff disks, e.g. if they decide to use integral bladed disks. (Experimentalists at the engine companies have also observed large blade to blade scatter and reported that the mass spring models did not predict this behavior.)

RECOMMENDATIONS

Several things could be done to make the linear mistuning code more efficient, more accurate, or more convenient. The primary ones are:

1. Modify the input data so that the disk modes could be calculated using cyclic symmetric boundary conditions in EAL. Currently, LMCC requires that the modes of the disk be calculated using a model of the full disk.

2. Add aerodynamic coupling between the blades. Currently, only blade and disk modal damping are included. During a NASA review, this option was not judge to be very important since most NASA applications correspond to very short stiff blades.

3. Modify the input preprocessor so that LMCC is compatible with other finite element codes. Currently, it only works with EAL or SPAR programs.

Nonlinear constraints could also be added to the formulation. For example, with appropriate modifications LMCC could handle shroud friction constraints in a very efficient manner.

Lastly, LMCC could be a very useful tool in assessing various strategies for actively controlling bladed disk response. The reason for this is that its structural fidelity would allow the researcher to quantitative assess the effect on system response of putting actuators at various locations on the disk and blades.

REFERENCES

1. J. H. Griffin, and M. T. Yang, "Exploring How Shroud Constraints Can Affect Vibratory Response in Turbomachinery," *Proceedings of the Advanced Earth-to-Orbit Propulsion Technology Conference*, 1992, pp 569-578.

2. M. T. Yang, J. H. Griffin, and L. Kiefling, "Mistuned Vibration of Bladed Disk Assemblies: A Reduced Order Approach," *Proceedings of the Advanced Earth-to-Orbit Propulsion Technology Conference*, 1994, pp 451-455.

Appendix A: Summary Report

EXECUTIVE SUMMARY

A reduced order approach is introduced that can be used to predict the steady-state response of mistuned bladed disks. This approach directly takes results from a finite element analysis of a tuned system and, based on the assumption of rigid blade base motion, constructs a computationally efficient mistuned model with a reduced number of degrees of freedom. Based on a comparison of results predicted by different approaches it is concluded that: the reduced order model displays structural fidelity comparable to that of a finite element model of the entire bladed disk system with significantly improved computational efficiency; and under certain circumstances both the finite element model and the reduced order model predict quite different response from simple spring-mass models.

INTRODUCTION

The resonant amplitudes of turbine blades tend to be sensitive to minor variations in the blades' properties. It is realized that, because of the rotational periodicity of its geometry, a bladed disk usually has natural frequencies that are clustered in narrow ranges. When the natural frequencies of a system are close together, slight variations in the system's structural properties can cause large changes in its modes, and, consequently, its dynamic response. The sensitivity of a bladed disk's dynamic response to small variations in the frequencies of the blades is referred to in the literature as the *blade mistuning* problem and has been studied extensively, for examples refer to Dye and Henry (1969), Ewins (1988), Fubunmi (1980), Griffin and Hoosac (1984), or Ottarsson and Pierre (1993). It is important to understand mistuning since it can result in large blade to blade variations in the vibratory response and the high response blades can fail from high cycle fatigue.

Much of the work that has been done in mistuning utilizes spring-mass models to represent bladed disks in order to reduce the number of degrees of freedom and to make the problem computationally tractable, for examples refer to the previously cited papers. The model's parameters, such as the mass and the spring constants, are chosen in an ad

hoc manner and one must question the ability of such simple models to accurately represent such complex systems. While some attempt has been made to corroborate the accuracy of spring-mass models by comparing predictions with specific test data, for example Griffin (1988), such work is relatively scarce.

Efforts have been made to develop more structurally accurate models for bladed disks by using plate elements to represent the disk and beam elements to represent the blades, for examples refer to Kaza and Kielb (1984), and Rzadkowski's two papers in (1994). While there can be blade configurations for which the beam representation may be adequate, plate, thick shell, and even solid elements are often needed to represent modern low aspect ratio blades. The finite element method could be a possible choice to accurately model a whole bladed disk, but it is recognized that the time cost and the storage space required to run these programs would be prohibitively high. For example, one could imagine using the Monte-Carlo approach of Griffin and Hoosac (1984) with detailed finite element models of the entire mistuned bladed disk. Such an approach would involve the analyses of hundreds of mistuned disks in order to determine the statistical variations in the blades' vibratory response. Clearly, such computations are currently beyond the capabilities of even super computers and would be hardly suitable for use as a design tool. Furthermore, because of the extremely large number of degrees of freedom involved and the closeness of the natural frequencies, one must question if such results would even be numerically accurate.

The limitations associated with spring-mass and beam models and the direct finite element approach motivate us to consider the possibility of developing a new model for analyzing mistuned bladed disks. Our goal is to develop a methodology that will directly take the results from a finite element analysis of a tuned system and construct a computationally efficient mistuned model with a reduced number of degrees of freedom. The intent is that the approach will display structural fidelity comparable to a finite element model and computational efficiency more comparable to that of a spring-mass model.

APPROACH FOR REDUCING THE NUMBER OF DEGREES OF FREEDOM

In the study of the steady-state response of complex structures, one widely used analytical approach is the *receptance method*, Bishop and Johnson (1960). The receptance method is based on the observation that the dynamic response of every

substructure is determined by how it interacts with its environment at its boundaries. If the substructure interacts with its environment only at limited areas, it is convenient to express the degrees of freedom of the entire substructure in terms of the degrees of freedom of its interfaces. The benefit of this method is that when several substructures interact with each other, it is only necessary to solve for the degrees of freedom associated with the interfaces. Once the degrees of freedom of the interfaces are determined the response of all substructures and, consequently, the whole structure may be calculated. To apply the receptance method to the mistuned bladed disk, it is divided into two substructures — the disk (Figure 1) and the blades (Figure 2). Modal analysis is then used to determine the substructures' behavior in terms of the degrees of freedom of the interfaces. However, the receptance method has two shortcomings:

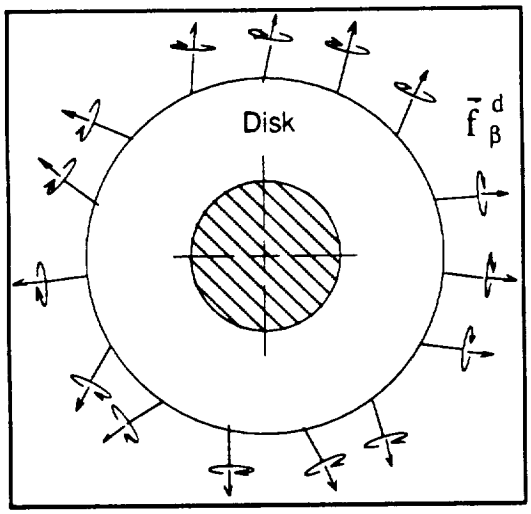

Figure 1: Disk substructure

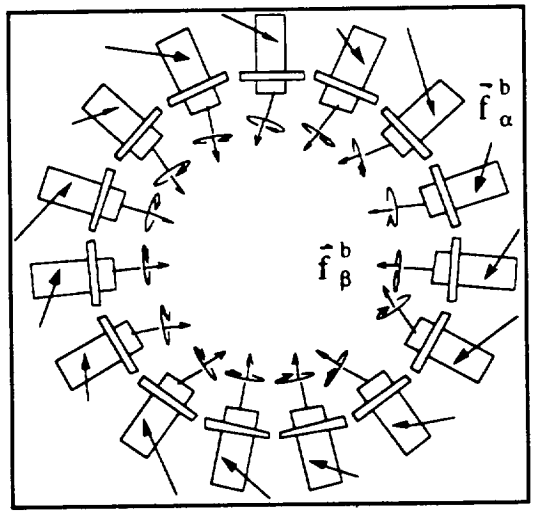

Figure 2: Blade substructure

1. The substructures' modes have to be free at the disk-blade interfaces in order to be admissible. This works reasonably well for the disk since the blades provide relatively little constraint at its rim and, consequently, only a few families of disk modes are required to represent its response. However, it is undesirable to use the free-free blade model. Because blades generally vibrate close to the clamped-free condition, a large number of the free-free modes are needed to achieve a good representation of its vibratory response.

2. A direct application of the receptance method results in a formulation with a reduced number of degrees of freedom. However, depending on the number of nodes at the blade interface, the number can still be quite large, especially if solid elements are used to model the blade's neck. Since it is undesirable to restrict the

approach to blade models with only a few nodes at the disk-blade interface, the receptance method needs to be modified in order to make it even more efficient. This is done using the following simplifying assumption.

It is assumed that the disk-blade interfaces undergo rigid body type translations and rotations. The blade vibration is then determined as a combination of blade base motion and clamped-free blade modes. As will be shown, this approach results in a formulation that has a relatively small number of degrees of freedom (six times the number of blades) and is consequently, computationally efficient. In addition, since the blade's response is represented in terms of its clamped-free modes its response can be quickly characterized with only a few modes.

MATHEMATICAL FORMULATION

Disk Equation

If the disk substructure is subjected to a harmonic excitation, its response is given by the receptance matrix $\mathbf{R}$, i.e.,

$$\begin{Bmatrix} \bar{u}^d_\alpha \\ \bar{u}^d_\beta \end{Bmatrix} = \begin{bmatrix} \mathbf{R}^d_{\alpha,\alpha} & \mathbf{R}^d_{\alpha,\beta} \\ \mathbf{R}^d_{\beta,\alpha} & \mathbf{R}^d_{\beta,\beta} \end{bmatrix} \begin{Bmatrix} \bar{f}^d_\alpha \\ \bar{f}^d_\beta \end{Bmatrix} \tag{1}$$

where $\bar{u}^d$, $\bar{f}^d$, and $\mathbf{R}^d$ are the displacement, the external force, and the receptance associated with the disk. The subscript α denotes the group of nodes that do not interact with other substructures and the subscript β denotes the group of nodes that reside at the disk-blade interfaces. Since the only external forces on the disk are the interactive forces at the disk-blade interfaces

$$\bar{f}^d_\alpha = \bar{0} \tag{2}$$

Equations (1) and (2) imply that

$$\bar{u}^d_\beta = \mathbf{R}^d_{\beta,\beta} \; \bar{f}^d_\beta \tag{3}$$

To formulate the disk equation in a more reduced order form, i.e., a formulation with six degrees of freedom per interface, the following two relations are introduced

$$\vec{u}_\beta^d \approx \mathbf{Q}_{\beta,o}^d \, \vec{u}_o^d \tag{4}$$

$$\vec{f}_o^d = \Sigma_{o,\beta}^d \, \vec{f}_\beta^d \tag{5}$$

where $\vec{u}_o^d$ is a vector whose components are the six equivalent rigid body-type motions of the disk at the interfaces and $\vec{f}_o^d$ is the resultant forces on the disk at the interfaces. $\mathbf{Q}_{\beta,o}^d$ is the geometric relation between $\vec{u}_\beta^d$ and $\vec{u}_o^d$ and $\Sigma_{o,\beta}^d$ is the geometric relation between $\vec{f}_o^d$ and $\vec{f}_\beta^d$. The inverse relations of equations (4), and (5) are

$$\vec{u}_o^d = \mathbf{Q}_{\beta,o}^{d\,+} \, \vec{u}_\beta^d \tag{6}$$

$$\vec{f}_\beta^d = \Sigma_{o,\beta}^{d\,+} \, \vec{f}_o^d \tag{7}$$

where $\mathbf{Q}_{\beta,o}^{d\,+}$ and $\Sigma_{o,\beta}^{d\,+}$ are the generalized inverses of the matrices $\mathbf{Q}_{\beta,o}^d$ and $\Sigma_{o,\beta}^d$. Their expressions are

$$\mathbf{Q}_{\beta,o}^{d\,+} = \left(\mathbf{Q}_{\beta,o}^{d\,T} \mathbf{Q}_{\beta,o}^d \right)^{-1} \mathbf{Q}_{\beta,o}^{d\,T} \tag{8}$$

$$\Sigma_{o,\beta}^{d\,+} = \Sigma_{o,\beta}^{d\,T} \left(\Sigma_{o,\beta}^d \, \Sigma_{o,\beta}^{d\,T} \right)^{-1} \tag{9}$$

In essence, equations (6) and (7) state that $\vec{u}_o^d$ is the least squares fit of $\vec{u}_\beta^d$ and $\vec{f}_\beta^d$ is the non-self-equilibrated forces estimated from $\vec{f}_o^d$. There are many possible choices of the distributed force $\vec{f}_\beta^d$. The reason that only the non-self-equilibrated forces were used is that, because of *Saint Venant's Principle*, the self-equilibrated forces die off quickly away from the interfaces and their global effect on the system should be relatively small. Substituting equations (6) and (7) into equation (3), results in the reduced order receptance formulation for the disk

$$\vec{u}_o^d = \mathbf{R}_{o,o}^d \, \vec{f}_o^d \tag{10}$$

where

$$\mathbf{R}^{d}_{o,o} = \mathbf{Q}^{d}_{\beta,o}{}^{+}\ \mathbf{R}^{d}_{\beta,\beta}\ \Sigma^{d}_{o,\beta}{}^{+} \tag{11}$$

By applying standard modal analysis, the disk receptance $\mathbf{R}^{d}_{\beta,\beta}$ can be written as

$$\mathbf{R}^{d}_{\beta,\beta} = \sum_{j} \frac{\bar{\phi}^{d}_{j,\beta}\ \bar{\phi}^{d}_{j,\beta}{}^{T}}{m^{d}_{j}\left(\omega^{d}_{j}{}^{2} - \Omega^{2} + 2i\Omega\omega^{d}_{j}\zeta^{d}_{j}\right)} \tag{12}$$

where $\bar{\phi}^{d}_{j}$ is the j^{th} disk mode, and m^{d}_{j}, ζ^{d}_{j}, and ω^{d}_{j} are the modal mass, modal damping ratio, and natural frequency of the j^{th} disk mode. Combining equations (11) and (12), the reduced order disk receptance can be written as

$$\mathbf{R}^{d}_{o,o} = \sum_{j} \frac{\bar{\phi}^{d}_{j,o}\ \bar{\phi}^{d}_{j,o}{}^{T}}{m^{d}_{j}\left(\omega^{d}_{j}{}^{2} - \Omega^{2} + 2i\Omega\omega^{d}_{j}\zeta^{d}_{j}\right)} \tag{13}$$

where $\bar{\phi}^{d}_{j,o}$, the j^{th} reduced order disk modes, is written as

$$\bar{\phi}^{d}_{j,o} = \mathbf{Q}^{d}_{\beta,o}{}^{+}\ \bar{\phi}^{d}_{j,\beta} \tag{14}$$

Blade Equation

Consider a single blade whose base is constrained to move in a plane undergoing small, harmonic translations and rotations. Let $\bar{u}^{b}_{o}$ be the six-degree-of-freedom displacement vector of the blade base and, again, denote the group of nodes that do not interact with the disk by the subscript α and the group of nodes that reside at the interface by β. The receptance equation for the blade can be written as

$$\bar{u}^{b}_{\alpha} - \mathbf{Q}^{b}_{\alpha,o}\,\bar{u}^{b}_{o} = \mathbf{R}^{b}_{\alpha,\alpha}\left(\bar{f}^{b}_{\alpha} + \Omega^{2}\,\mathbf{M}^{b}_{\alpha,\alpha}\,\mathbf{Q}^{b}_{\alpha,o}\,\bar{u}^{b}_{o}\right) \tag{15}$$

$$\bar{u}^{b}_{\beta} = \mathbf{Q}^{b}_{\beta,o}\ \bar{u}^{b}_{o} \tag{16}$$

where Ω is the excitation frequency. $\bar{u}^{b}$, $\bar{f}^{b}$, and $\mathbf{R}^{b}$ are the displacement, the external force, and the receptance associated with the blade. $\mathbf{M}^{b}_{\alpha,\alpha}$ is the blade mass matrix

associated with the group-α nodes. $\mathbf{Q}^b_{\alpha,o}$ and $\mathbf{Q}^b_{\beta,o}$ are geometric functions such that $\mathbf{Q}^b_{\alpha,o}\,\bar{u}^b_o$ and $\mathbf{Q}^b_{\beta,o}\,\bar{u}^b_o$ describe the motion of the entire blade provided that the blade follows the motion of its base and does not deform. The term $\Omega^2\,\mathbf{M}^b_{\alpha,\alpha}\,\mathbf{Q}^b_{\alpha,o}\,\bar{u}^b_o$ in the right hand side of equation (15) describes the inertial force introduced by the blade base motion. Rearranging equation (15), the motion of the group-α nodes $\bar{u}^b_\alpha$ can be expressed in terms of the external excitation force $\bar{f}^b_\alpha$ and the blade base motion $\bar{u}^b_o$, i.e.,

$$\bar{u}^b_\alpha = \mathbf{R}^b_{\alpha,\alpha}\;\bar{f}^b_\alpha + \left(\Omega^2\,\mathbf{R}^b_{\alpha,\alpha}\,\mathbf{M}^b_{\alpha,\alpha} + \mathbf{I}\right)\mathbf{Q}^b_{\alpha,o}\,\bar{u}^b_o \tag{17}$$

From modal analysis, the receptance $\mathbf{R}^b_{\alpha,\alpha}$ can be written as

$$\mathbf{R}^b_{\alpha,\alpha} = \sum_j \frac{\bar{\phi}^b_{j,\alpha}\;\bar{\phi}^{b\,T}_{j,\alpha}}{m^b_j\left(\omega^{b\,2}_j - \Omega^2 + 2i\Omega\omega^b_j\zeta^b_j\right)} \tag{18}$$

where $\bar{\phi}^b_j$ is the j^{th} mode for a blade clamped at its base, and m^b_j, ζ^b_j, and ω^b_j are the modal mass, modal damping ratio, and natural frequency of the j^{th} blade mode.

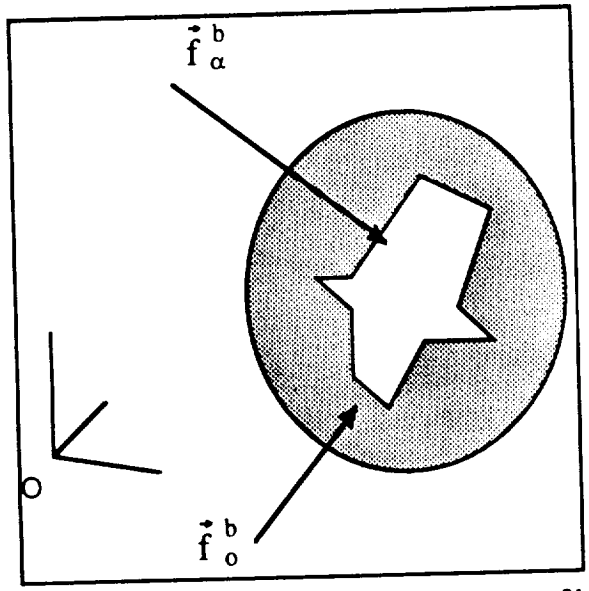

Figure 3: Forces acting on free body diagram of blade

The resultant force on the blade base, $\bar{f}^b_o$, is needed in order to assemble the entire system. To determine $\bar{f}^b_o$ consider the blade as an object which can move and deform in

space (Figure 3). The forces acting on the blade are the excitation force $\bar{f}_\alpha^b$ and the interactive force at the interface $\bar{f}_o^b$. Since linear and angular momentum have to be conserved, one can deduce that

$$\Sigma_o^b\left(-\Omega^2 \mathbf{M}^b \bar{u}^b\right) = \Sigma_o^b \bar{f}^b = \Sigma_{o,\alpha}^b \bar{f}_\alpha^b + \bar{f}_o^b \tag{19}$$

where Σ_o^b is a geometric function which calculates the resultant force and moment about the blade base O. Substituting equations (16) and (17) into equation (19), $\bar{f}_o^b$ can be expressed in terms of the blade base motion $\bar{u}_o^b$ and the external excitation $\bar{f}_\alpha^b$, i.e.,

$$\bar{f}_o^b = \mathbf{Z}_{o,o}^b \bar{u}_o^b + \mathbf{H}_{o,\alpha}^b \bar{f}_\alpha^b \tag{20}$$

where

$$\mathbf{Z}_{o,o}^b = -\Omega^2 \Sigma_o^b \mathbf{M}^b \mathbf{Q}_o^b - \Omega^4 \Sigma_{o,\alpha}^b \mathbf{M}_{\alpha,\alpha}^b \mathbf{R}_{\alpha,\alpha}^b \mathbf{M}_{\alpha,\alpha}^b \mathbf{Q}_{\alpha,o}^b \tag{21}$$

$$\mathbf{H}_{o,\alpha}^b = -\Omega^2 \Sigma_{o,\alpha}^b \mathbf{M}_{\alpha,\alpha}^b \mathbf{R}_{\alpha,\alpha}^b - \Sigma_{o,\alpha}^b \tag{22}$$

Equation (20) describes the relation between the interactive force $\bar{f}_o^b$, the blade base motion $\bar{u}_o^b$, and the external excitation $\bar{f}_\alpha^b$ for a single blade. Clearly, similar equations apply for all blades. In fact, equations (20), (21) and (22) describe the motions of all of the blades provided the vectors represent the collections of the corresponding vectors of individual blades and the matrices become block diagonal matrices with the corresponding matrices of individual blades at the diagonals.

Assembling the Substructures

Equations (10) and (20) describe the relations between the interactive forces and the motion of the interfaces for the disk and the blades respectively. Since there are four unknown vectors, $\bar{u}_o^d$, $\bar{f}_o^d$, $\bar{u}_o^b$, and $\bar{f}_o^b$ to be determined, there needs to be two additional constraints. The first is Newton's law of interactive forces, i.e.,

$$\bar{f}_o^d = -\bar{f}_o^b \tag{23}$$

The second one is Hooke's law which provides a constitutive relation at the interfaces, i.e.,

$$\bar{f}_o^d = \mathbf{K}_{o,o}\left(\bar{u}_o^d - \bar{u}_o^b\right) \tag{24}$$

where $\mathbf{K}_{o,o}$ is the stiffness matrix associated with the attachment at the disk-blade interfaces.[1] By solving equations (10), (20), (23), and (24) simultaneously, the four unknowns can be expressed in terms of the external excitation force $\bar{f}_\alpha^b$, i.e.,

$$\bar{u}_o^b = -\left(\mathbf{R}_{o,o}^d + \mathbf{K}_{o,o}^{-1}\right)\left[\mathbf{I} + \mathbf{Z}_{o,o}^b\left(\mathbf{R}_{o,o}^d + \mathbf{K}_{o,o}^{-1}\right)\right]^{-1}\mathbf{H}_{o,\alpha}^b \bar{f}_\alpha^b \tag{25}$$

$$\bar{f}_o^b = \left[\mathbf{I} + \mathbf{Z}_{o,o}^b\left(\mathbf{R}_{o,o}^d + \mathbf{K}_{o,o}^{-1}\right)\right]^{-1}\mathbf{H}_{o,\alpha}^b \bar{f}_\alpha^b \tag{26}$$

$$\bar{u}_o^d = -\mathbf{R}_{o,o}^d\left[\mathbf{I} + \mathbf{Z}_{o,o}^b\left(\mathbf{R}_{o,o}^d + \mathbf{K}_{o,o}^{-1}\right)\right]^{-1}\mathbf{H}_{o,\alpha}^b \bar{f}_\alpha^b \tag{27}$$

$$\bar{f}_o^d = -\left[\mathbf{I} + \mathbf{Z}_{o,o}^b\left(\mathbf{R}_{o,o}^d + \mathbf{K}_{o,o}^{-1}\right)\right]^{-1}\mathbf{H}_{o,\alpha}^b \bar{f}_\alpha^b \tag{28}$$

The vibration of the blades can then be easily derived by substituting equation (25) into equation (17).

Remarks on the Mathematical Approach

There are several advantages of using the reduced order formulation (equations (17) and (25)) to solve the blade mistuning problem:

1. The coefficient matrices $\mathbf{R}_{o,o}^d$, $\mathbf{Z}_{o,o}^b$, and $\mathbf{H}_{o,\alpha}^b$ are calculated from the substructures' modes. Since the frequency range is usually limited to a narrow range near a particular engine order crossing, only a few dominant modes need to be included in the calculation and, consequently, the computational cost is low.

[1] If the attachment is infinitely stiff, then (24) implies that the displacements in the blade and disk are equal, and, consequently, (24) becomes a continuity requirement.

2. For blade mistuning problems, the disk is treated as a cyclic symmetric structure. As a result, its modes can be calculated efficiently by applying cyclic symmetric boundary conditions on a disk segment corresponding to a single blade.

3. The most computationally intensive part of this approach lies in computing the inverse of the matrix $\left[\mathbf{I}+\mathbf{Z}^{b}_{o,o}\left(\mathbf{R}^{d}_{o,o}+\mathbf{K}^{-1}_{o,o}\right)\right]$ in equation (25). This is a square matrix with dimension six times the number of the blades. In many problems the rigidity of the disk is such that only three degrees of freedom are needed to describe the blade's motion at its base, two rotations and translation normal to the disk. In either case the number of degrees of freedom are orders of magnitude smaller than for a finite element model for an entire mistuned bladed disk.

4. The reduced order method is especially computationally efficient when running Monte Carlo simulations of blade mistuning since the disk's modes and the nominal blade's modes need only be calculated once. The coefficient matrices associated with the blades $\left(\mathbf{Z}^{b}_{o,o}\right.$ and $\left.\mathbf{H}^{b}_{o,\alpha}\right)$ are calculated by changing the cantilever blade frequencies in the receptance calculation for each blade. On the other hand, a direct simulation using finite element models would require completely new calculations for each mistuned stage.

COMPARISON OF RESULTS

A computer code named LMCC (Linear Mistuning Computer Code) has been developed based on the reduced order approach. A test problem was developed, Figure 4, and analyzed using: 1) modal summation based on a direct finite element analysis, 2) LMCC, and 3) the mass-spring model of Griffin and Hoosac (1984) as depicted in Figure 5. The response of the spring-mass model is determined using the computer code BLDVIB. The vibratory response of more than one hundred different resonant crossings have been examined of which the examples presented in this section are representative.

The geometry of the test problem was chosen so that the following requirements were satisfied:

1. The disk and the nominal blade have natural frequencies that are representative of a turbo-pump. Both the blades and disk are assumed to have material properties associated with a super nickel alloy.

2. The test problem represents a realistic three dimensional structure with low aspect ratio, plate-like blades. A test problem consisting of beam-type blades would not be appropriate since a goal is to check the validity of the simplifying constraint that the bases of the blades move as rigid bodies.

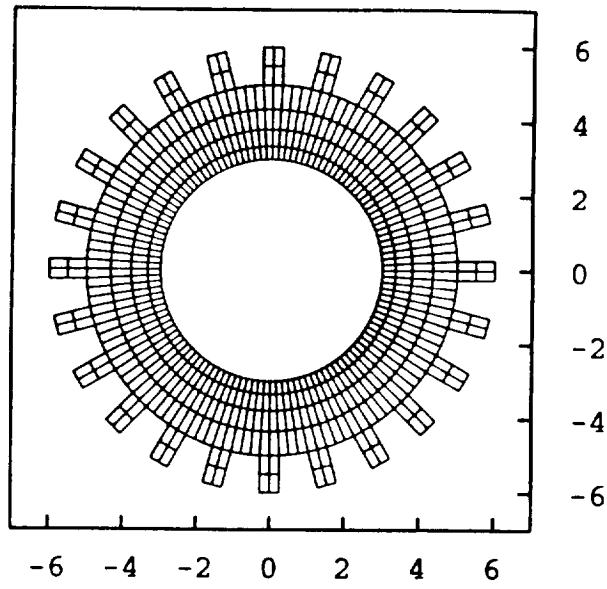

Figure 4: Finite element model of test problem

3. The entire system does not have too many degrees of freedom. As a result the entire bladed disk can be directly analyzed by finite elements without expending too much computational time or having numerical stability problems.

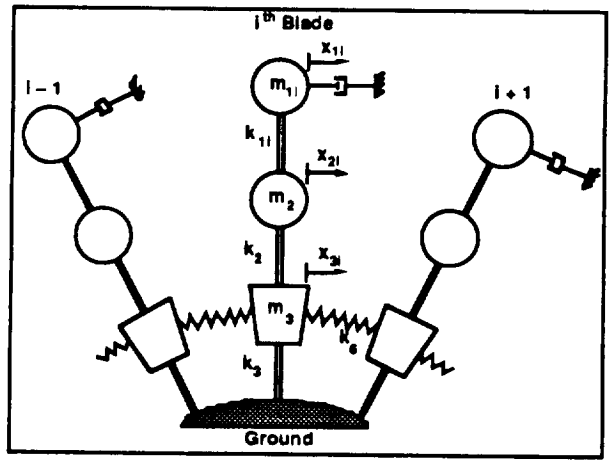

Figure 5: Spring-mass model used by Hoosac and Griffin

There are still several parameters of the reduced order model that need to be determined before the algorithm can be implemented. The attachment stiffness matrix $\mathbf{K}_{o,o}$ is set to infinity to represent the simplified geometry of the test problem. The other parameters that need to be determined are the damping ratios of the substructures' modes. It is assumed that both the blades and the disk have the same damping ratio. Its value is chosen so that the resonant response predicted by LMCC for the tuned system is the same as that predicted by the finite element method.

Tuned Response

First a comparison will be made between LMCC and the finite element method based on the natural frequencies of a tuned bladed disk. LMCC does not readily compute

natural frequencies. However, if the system is lightly damped they can be inferred by the system's resonant frequencies since they can be calculated using LMCC's forced response algorithm. Figure 6 shows a comparison of natural frequencies. The integer "j" refers to the engine order of the excitation which excites the j^{th} nodal diameter mode. Overall, the two methods agree reasonably well. However, the reduced order approach tends to predict slightly higher frequencies probably because of the assumption of rigid blade base motion which tends to over constrain the system. Note that the reduced order model represents the structure's response over a wide range of frequencies and nodal diameters. Results from the spring-mass model are not shown since the natural frequencies of the tuned system are part of the input parameters to the method and not calculated results.

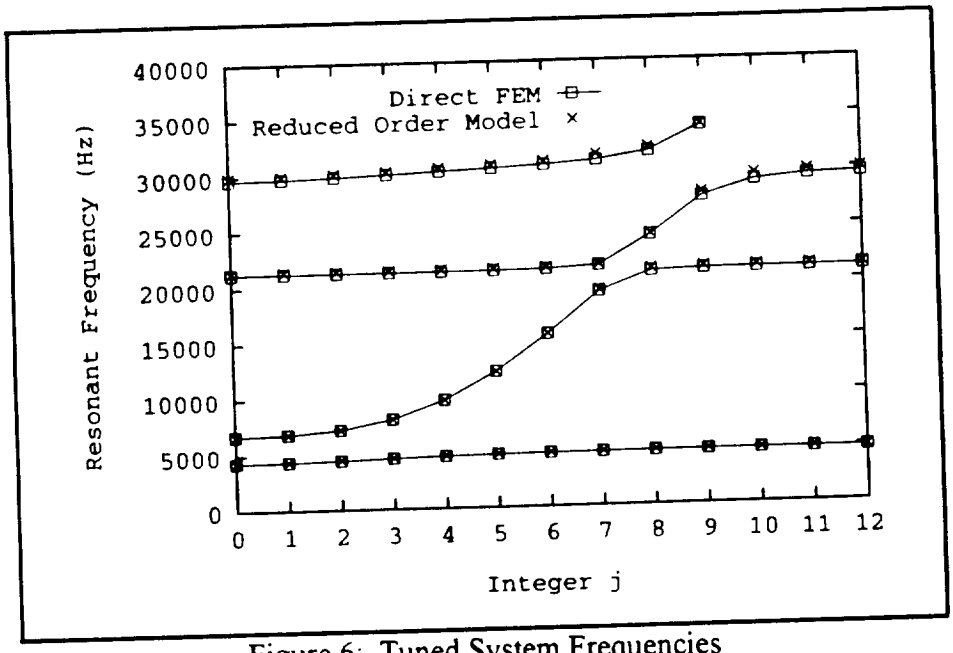

Figure 6: Tuned System Frequencies

The nominal properties of the spring-mass model were calculated using the approach given by Griffin (1988). Initially, the spring-mass model predicted a spurious second mode which had to be eliminated by varying some of the parameters. Figure 7 shows representative response curves of the tuned system as predicted by the three different methods. For this particular case, the bladed disk is subjected to a fourth engine order excitation and the blades vibrate predominantly in their first bending mode. It appears that the three curves agree well with each other though the response predicted by the reduced order model is at a slightly higher frequency.

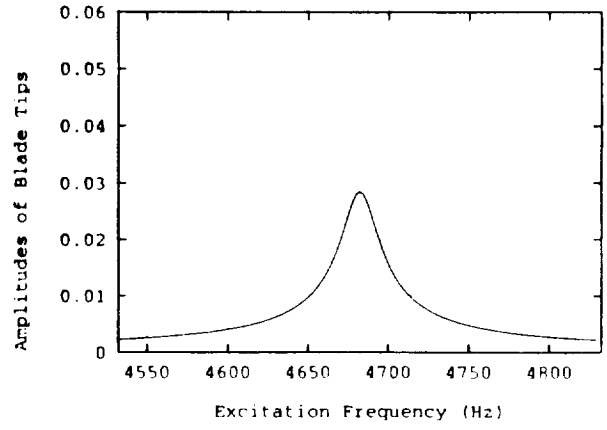

a. Finite element baseline

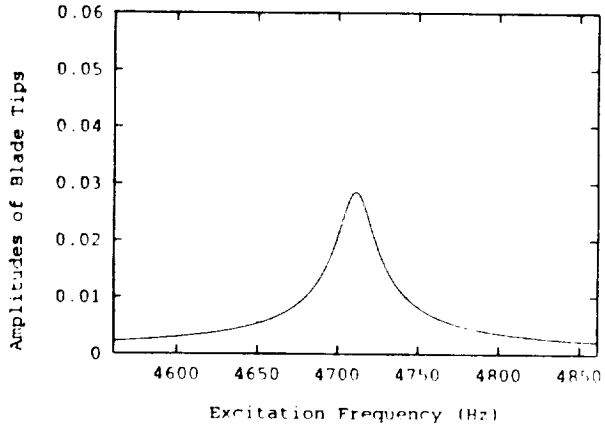

b. Reduced order model

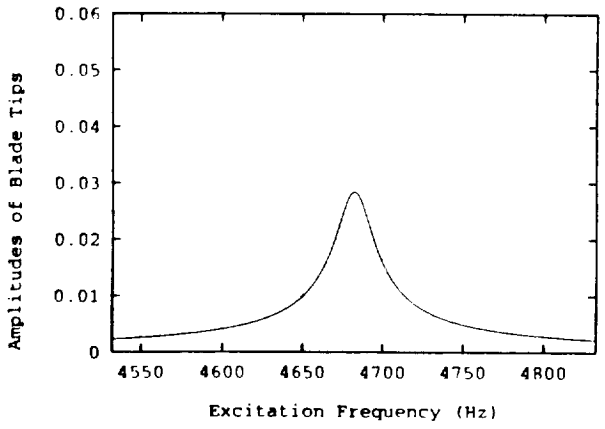

c. Spring-mass model

Figure 7: Tuned response curves

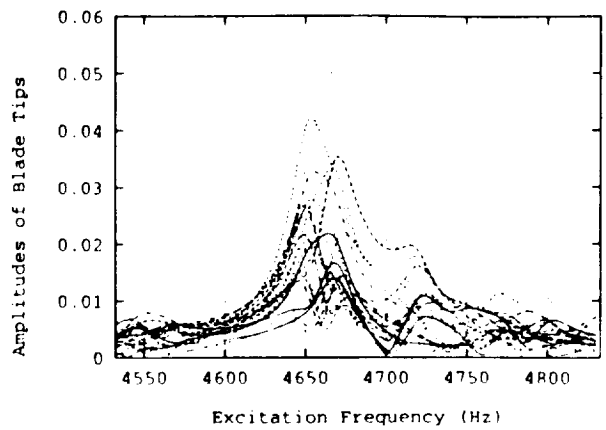

a. Finite element baseline

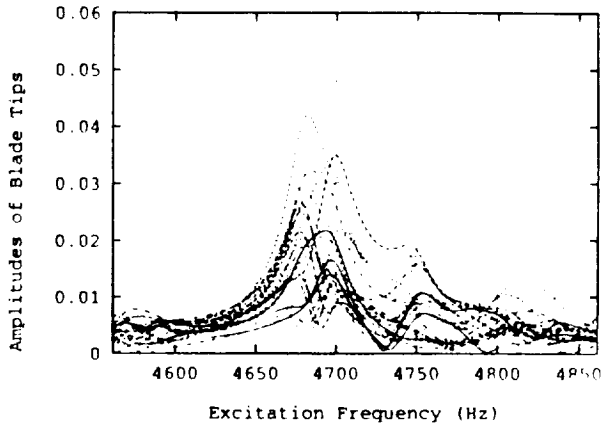

b. Reduced order model

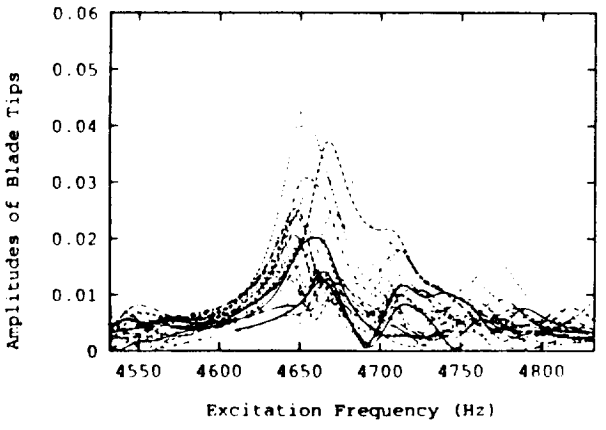

c. Spring-mass model

Figure 8: Mistuned response curves for blades in first bending

Mistuned Response

The finite element model is mistuned by varying the elastic modulus of the material in each blade. This same effect is simulated in LMCC by changing the natural frequencies of each blade when calculating its receptance. In the case of BLDVIB the stiffness, k_{1i}, of each blade was altered to produce the same frequency distribution. Figure 8 shows representative response curves of the blades as predicted by the three methods. In this case the bladed disk is subjected to a fourth engine order excitation and the blades predominantly vibrate in their first bending mode. Clearly, the agreement of all three methods is quite good. In general, it was observed that the reduced order model and the spring-mass model give comparable results when the blades respond predominately in their first bending modes.

Figure 9 depicts representative response curves when the blades are excited in their first torsional mode. It is clear from the plots that the reduced order model works much better than the spring-mass model in representing the response of the system. This case differs from the bending mode case in that the disk is effectively much stiffer. This stiffness effect is discernible from the fact that the percentage change in the frequencies of the four and five diameter modes of the tuned system (Figure 6) is an order of magnitude smaller for the torsional modes than the first bending modes. For a stiff disk, the spring-mass model predicts that the blades essentially respond as isolated mistuned blades on a rigid foundation. However, both the finite element and LMCC results indicate that there is still significant interaction between the blades that results in complex system dynamics that is not captured by the simple spring-mass models.[2]

Limitations of the Reduced Order Model

Additional simulations were made with both thicker and thinner disks. In general, finite element and LMCC results agreed quite well except for one case. Figure 10 shows the response curves predicted by the three different models for a bladed disk when the thickness of the disk is halved. In the case in question, the tuned system has a response which is similar to the frequency veering that is observed for the second and third modes when j equals seven in Figure 6. As a result, the bladed disk has two families of modes that are close together and that respond to the excitation. Because of the closeness of the

[2] Simulations were also made of the response of the mistuned system in first bending with a stiffer disk. In this case all three methods predicted that the blades would respond as isolated blades. Again, the spring-mass model worked quite well for first bending.

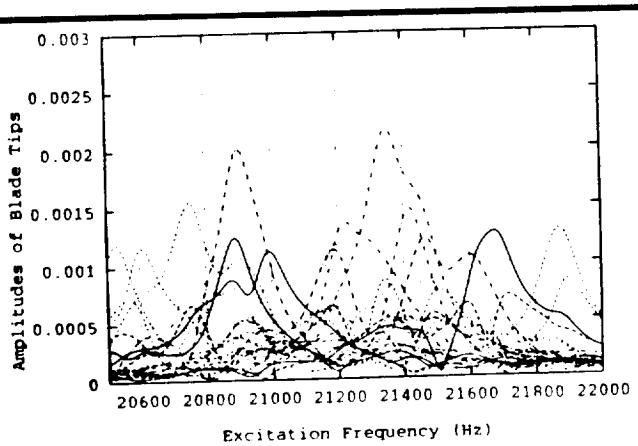

a. Finite element baseline

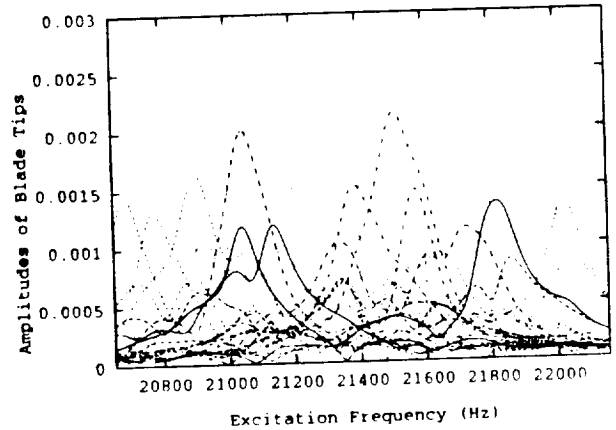

b. Reduced order model

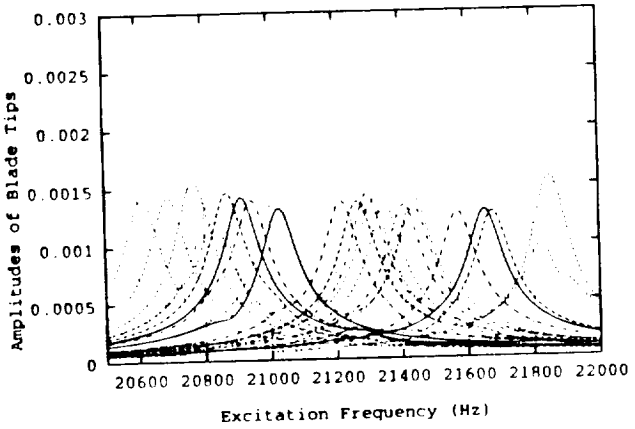

c. Spring-mass model

Figure 9: Mistuned response curves for blades in first torsion

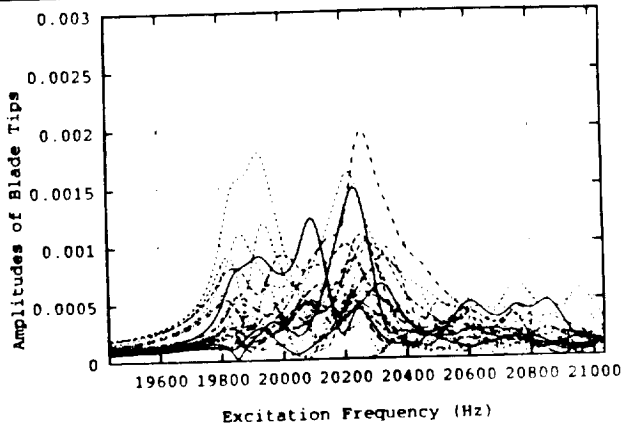

a. Finite element baseline

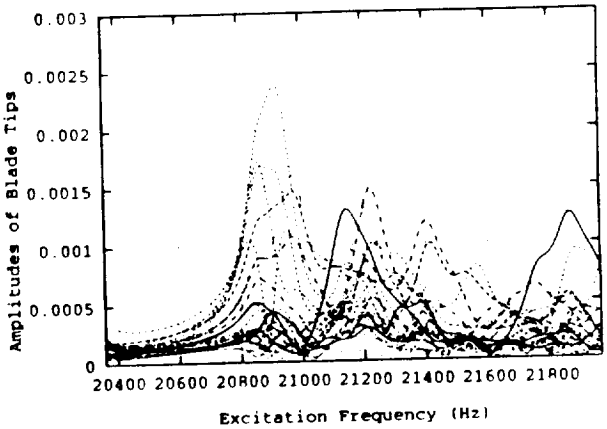

b. Reduced order model

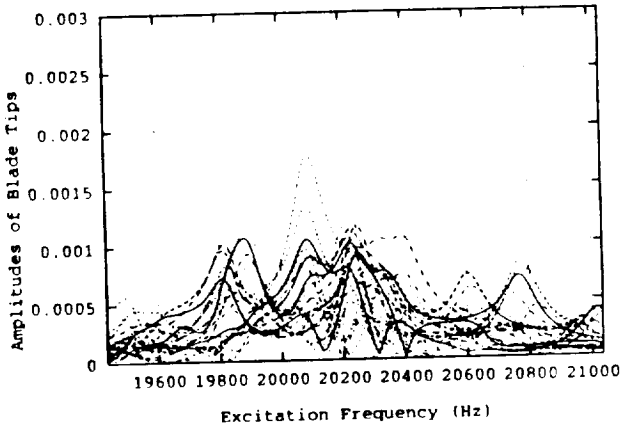

c. Spring-mass model

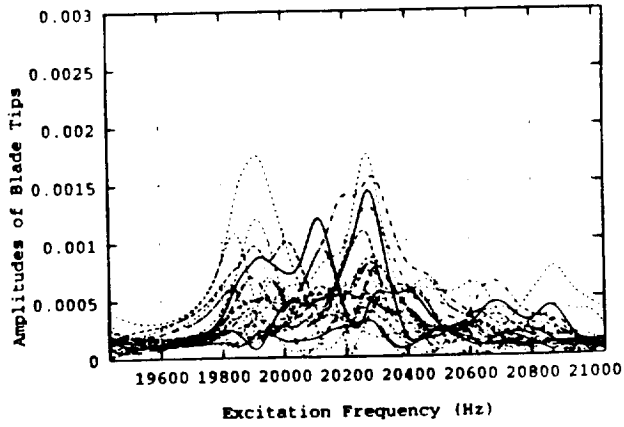

d. Reduced order model using Adjusted K_{00}

Figure 10: Mistuned response curves for coupled disk and torsion modes

frequencies, the resulting modes contain significant amounts of both disk and torsional blade response. It appears that neither the reduced order model nor the spring-mass model successfully predict the correct results. One problem with the LMCC model is that it does not predict the separation in the frequencies of the two families of modes very accurately. This problem was addressed by introducing a finite value of the blade attachment stiffness matrix, $\mathbf{K}_{oo}$, so that the frequency difference for the tuned system's response was the same as that of the finite element model. Figure 10(d) shows the response curves predicted by the reduced order model when the attachment stiffness has been adjusted. The results from the reduced order model agree somewhat better with the finite element results, but not as well as in the other cases examined.

Execution Time Comparison

There are two principal advantages of the reduced order model approach which lead to increased computational efficiency. The first is that the number of degrees of freedom that must be determined (three or six per blade) in the forced response analysis is independent of the refinement of the finite element model of the blade and disk models that are used to calculate its input. Thus, LMCC is especially efficient when compared to a direct finite element solution of a bladed disk that has a large number of elements. Secondly, the most computationally expensive part of the calculation with LMCC is in calculating the modes of the clamped blade and tuned disk using finite elements. Since this needs to be done only once, LMCC becomes progressively more efficient when more mistuned bladed disks are simulated in a specific Monte Carlo analysis. An estimate of the relative run times of LMCC and a finite element analysis using modal superposition for a representative case indicates that LMCC would be two to three orders of magnitude faster for a one hundred bladed disk simulation.

CONCLUSIONS

A new reduced order approach has been developed for analyzing the forced response of mistuned bladed disks. The reduced order model is based on the idea of decomposing the bladed disk into substructures and representing the response in terms of the degrees of freedom associated with their interfaces. It further assumes that the blade bases undergo rigid body-type motions. The blade vibration may then be expressed as a combination of blade base motion and cantilever blade modes. This approach results in only six

equivalent degrees of freedom, three rotations and three translations, at each disk-blade interface. Because of the reduction in the number of unknowns, the reduced order model provides a formulation which can be solved efficiently by computers. An advantage of this formulation is that the reduced order model is directly calculated from finite element analyses of a single clamped blade and a tuned disk without any additional ad hoc assumptions.

Comparisons of results from direct finite element simulations and the reduced order model indicate that, in general, the reduced order model agrees quite well with the finite element baseline. An exception to this agreement occurred when modes from two different families (one predominately blade modes and one predominately disk modes) were close in frequency and excited simultaneously. Comparisons were also made with results from spring-mass models. The spring-mass models predicted good results when the blades were responding predominately in first bending, but did not predict the response when the disk was stiff and the blades were responding predominately in first torsion.

REFERENCES

Bishop, R. E. D. and Johnson, D. C., 1960, *Mechanics of Vibration*, Cambridge University Press.

Dye, R. C. F. and Henry, T. A., 1969, "Vibration Amplitudes of Compressor Blades Resulting From Scatter in Blade Natural Frequencies," Transactions of the ASME, pp. 182-188.

Ewins, D. J., 1988, "Structural Dynamic Characteristics of Bladed Assemblies," *ALGOR Manual on Aeroelasticity in Axial-Flow Turbomachines*, Vol. 2, Specialized Printing Service Limited, Loughton, pp. 15-1 to 15-37.

Fabunmi, J. A., 1980, "Forced Vibrations of a Single Stage Axial Compressor Rotor," *Journal of Engineering for Power, Transactions of the ASME*, Vol. 102, pp. 322-328.

Griffin, J. H. and Hoosac, T. M., 1984, "Model Development and Statistical Investigation of Turbine Blade Mistuning," *Journal of Vibration, Acoustics, Stresses, and Reliability in Design, Transactions of the ASME*, Vol. 106, pp. 204-210.

Griffin, J. H., 1988, "On Predicting the Resonant Response of Bladed Disk Assemblies," *ASME Journal of Engineering for Gas Turbines and Power*, Vol. 110, pp. 45-50.

Kaza, K. R. V. and Kielb, R. E., 1984, "Flutter of Turbofan Rotors with Mistuned Blades," *AIAA Journal*, Vol. 22, No. 11.

Ottarsson, G. and Pierre, C., 1993, "A Transfer Matrix Approach to Vibration Localization in Mistuned Blade Assemblies," ASME Report No. 93-GT-115, presented at the International Gas Turbine and Aeroengine Congress and Exposition, Cincinnati, Ohio, May 24-27.

Rzadkowski, R., 1994, "The General Model of Free Vibrations of Mistuned Bladed Discs, Part I: Theory," *Journal of Sound and Vibration*, Vol. 173, No. 3, pp. 377-393.

Rzadkowski, R., 1994, "The General Model of Free Vibrations of Mistuned Bladed Discs, Part II: Numerical Results," *Journal of Sound and Vibration*, Vol. 173, No. 3, pp. 395-413.

Wagner, L. F., 1993, "Vibration Analysis of Grouped Turbine Blades," Ph.D. Thesis, Carnegie Mellon University, Pittsburgh, PA.

APPENDIX B: USER MANUAL FOR LMCC

INTRODUCTION

LMCC (Linear Mistuning Computer Code) is a FORTRAN program designed to solve for the steady-state vibratory response of mistuned bladed disk assemblies. It is the implementation of the Reduced Order Algorithm developed by Yang and Griffin. This algorithm directly takes the results from a finite element analysis of nominal substructures (i.e., disk and blade) to construct a model for a mistuned bladed disk. With blade bases being assumed moving rigidly, it constructs a reduced order system of equations which can be computationally efficiently solved.

In the following descriptions of the procedure for running LMCC, it is assumed that the reader may refer to the example files provided with the LMCC code.

CONTROL FLOW OF LMCC

LMCC is composed of several subprograms. Figure 1 shows the control flow of LMCC. The names of the subprograms under the UNIX system are shown in the brackets. Block 1 is the interface between EAL and LMCC which rearranges the output data from EAL for the use of LMCC. Block 2 calculates the frequency independent properties of the disk and the nominal blade. Block 3 helps users to specify the stiffness of the disk-blade attachment and generates the mistuned natural frequencies of the blades. Block 4 utilizes the outputs from the previous blocks to calculate the forced response of the mistuned bladed disk and generate preliminary results from which the vibration of the disk and the blade can be calculated. Block 5 extracts the information from preliminary results to calculate and print out the nodal amplitudes of the blades.

An important rule to run LMCC is that the subprograms in the same block are mutually independent but are dependent of the results from the previous blocks.

Example 1. If a user wants to change the attachment stiffness of the disk-blade interface but keep analyzing the same set of blades after a certain run, he/she can just go back to Block 3 to run the subprogram [interface] and run [assembly] in Block 4 and [amplitude] in Block 5, consequently; he/she does not have to run [ranbld] in Block 3 or any subprogram in Blocks 1 and 2.

Example 2. After a certain run, if a user decides that he/she wants to see the amplitudes of certain blade nodes which were not printed out previously, he/she only needs to rerun the subprogram [amplitude].

Example 3. To run a Monte Carlo simulation for the mistuned analysis of a particular nominal design, one can run LMCC according to the following steps:

Step 1. Run EAL for the disk and the nominal blade.

Step 2. Run [eal_disk] and [eal_blade].

Step 3. Run [disk] and [blade].

Step 4. Run [interface].

Step 5. Run [ranbld] to generate mistuned blade frequencies. Giving different seeds to the random number generator will produce different sets of blades.

Step 6. Run [assembly].

Step 7. Run [amplitude].

Step 8. If necessary, rename the output file of [amplitude] to save the result of a particular stage. The default output file name is "lmcc.out.amplitude." If this file is not renamed, the next run of [amplitude] will overwrite the file.

Step 9. Change the seed of [ranbld] and go back to Step 5.

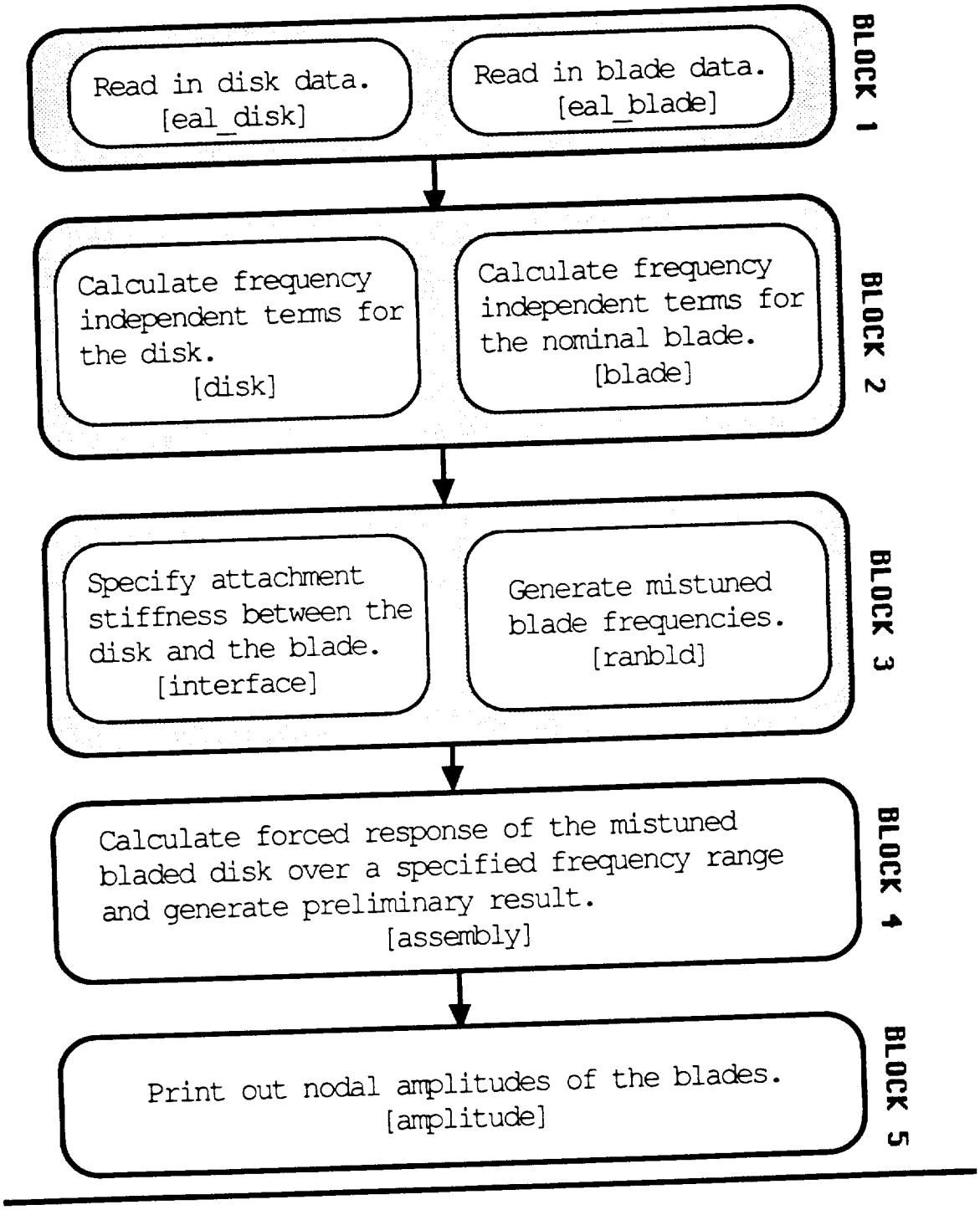

Figure 1 Control Flow of LMCC

INSTALLATION OF LMCC

To install LMCC under UNIX systems, one can do the following:

1. Store all of the LMCC source codes in a directory and *cd* to this directory.
2. Key in *make* to create the executables automatically. You can also build LMCC manually by keying in the following commands:

```
f77 -o eal_disk eal_disk.f
f77 -o eal_blade eal_blade.f
f77 -o disk disk_0.f disk_1.f disk_2.f dmatrix.f zmatrix.f
f77 -o blade blade_0.f blade_1.f blade_2.f dmatrix.f zmatrix.f
f77 -o interface interface.f
f77 -o ranbld ranbld_0.f ranbld_1.f
f77 -o assembly -O assembly.f dmatrix.f zmatrix.f
f77 -o amplitude -O amplitude.f
```

   Notice: Since LMCC is quite computationally intensive, users are encouraged to compile the optimized executables. However, due to problems from some vendors, the optimization should be used with care. For example, on Silicon Graphic workstations running IRIX 5.2, using MIPS FORTRAN 77 to compile *ranbld* with optimization can cause the executable to work improperly.

3. Correctly set the PATH environment so that the executables of LMCC can be found by the system.

INPUT FILES FOR EAL

Before running LMCC, the finite element analysis by EAL has to be done first. The format of the EAL input files for the disk and the (nominal) blade are as follows:

Input File for the Disk

The input file for the disk must contain the following statements (in addition to the standard input data, for instance, geometry, element type, etc.) This version of LMCC requires that a modal analysis of the entire disk is made, that is, not a cyclic symmetric segment.

```
          .
          .
          .
*XQT EIG
          .
          .
          .
$ END OF EIG
*XQT DCU
 PRINT 1 JLOC
 PRINT 1 VIBR MODE
          .
          .
          .
$ END OF DCU
          .
          .
          .
```

Input File for the (Nominal) Blade

The input file for the blade must contain the following statements (in addition to the standard input data, for instance, geometry, element type, etc.)

```
          .
          .
          .
*XQT M
          .
          .
          .
$ END OF M
          .
          .
          .
*XQT EIG
 RESET M=CEM
          .
          .
          .
$ END OF EIG
*XQT PS
*ONLINE=1
*FORMAT=2
 CEM
$ END OF PS
*XQT DCU
 PRINT 1 JLOC
 PRINT 1 VIBR MODE
          .
          .
          .
$ END OF DCU
          .
          .
          .
```

Notice

1. The execution sequence shown above should be strictly followed. Otherwise, LMCC will indicate there is an error. The general rule is that the natural frequencies have to be printed out first (by EIG), then CEM matrix (by PS), then JLOC (by DCU), and finally VIBR MODE (by DCU).
2. LMCC needs the complete mass matrix of the nominal blade to calculate the forced response of the system. Since EAL can not print out the moments of inertia of the nodes while using lumped mass matrix (DEM), LMCC uses the consistent mass matrix (CEM). Therefore, when running EAL on the blade, one must use CEM for the analysis.
3. The joint locations (JLOC) and the natural modes (VIBR MODE) have to be put in Cartesian coordinates. LMCC will not work properly if they are specified in polar coordinates.

INPUT FILES FOR SUBPROGRAMS OF LMCC

To run the subprograms of LMCC, the associated input files have to be ready beforehand. There are eight input files corresponding to each of the subprograms indicated in Figure 1. The input files are named as *[subprogram name].in*. For example, the input file name for subprogram *eal_disk* is *eal_disk.in*. The input files provide information which are essential to the forced response analysis and will be read by the subprograms. The formats of the input files are as follows:

Example File 1: Input File for Subprogram *eal_disk* — *eal_disk.in*

The subprogram *eal_disk* functions as a interface between EAL and LMCC which reads the EAL ouput for the disk and reformat it for the input of LMCC.

```
1.0       0.0       0.0                 :record 1
0.0       1.0       0.0                 :record 2
0.0       0.0       1.0                 :record 3

0.866     -0.5      0.0                 :record 4
0.5       0.866     0.0                 :record 5
0.0       0.0       1.0                 :record 6
```

```
3                                       NDI:record 7
481                                     :record 8
482                                     :record 9
483                                     :record 10 (7+NDI)

0.0       5.0       0.0                 :record 11 (7+NDI+1)

10                                      :record 12 (7+NDI+2)

45                                      :record 13 (7+NDI+3)
12                                      :record 14 (7+NDI+4)
3         4         5                   :record 15 (7+NDI+5)
```

Explanation of Records

(1 to 3)

Matrix of direction cosines which transfers the disk coordinates to the first blade coordinates.

(4 to 6)

Matrix of direction cosines which transfers the ith blade coordinates to the (i+1)th blade coordinates.

(7)

NDI: Number of disk nodes per disk-blade interface.

(8 to 7+NDI)

Nodal numbers of disk nodes residing at the first disk-blade interface.

(7+NDI+1)

Position of the reference point O (in disk coordinates) associated with the first blade.

(7+NDI+2)

Nodal number difference between corresponding disk nodes residing at neighboring interfaces.

(7+NDI+3)

Number of disk modes to be stored in the library (for future use).

(7+ND+4)

Number of blades.

(7+ND+5)

Degrees of freedom of VIBR MODE printed out by DCU.

File *eal_blade.in* — Input File for Subprogram *eal_blade*

```
10                                      :record 1
```

```
3                                       NBI:record 2
1                                       :record 3
2                                       :record 4
3                                       :record 5 (2+NBI)

0.0       5.0       0.0                 :record 6 (2+NBI+1)

3         4         5                   :record 7 (2+NBI+2)
```

Explanation of Records

(1)

Number of blade modes to be stored in the library (for future use).

(2)

NBI: Number of blade nodes per disk-blade interface.

(3 to 2+NBI)

Nodal numbers of blade nodes residing at disk-blade interface.

(2+NBI+1)

Position of the reference point O (in blade coordinates).

(2+NBI+2)

Degrees of freedom of VIBR MODE printed out by DCU.

File *disk.in* — Input File for Subprogram *disk*

```
10                                      NDM:record 1
2                                       :record 2
3                                       :record 3
8                                       :record 4
9                                       :record 5
13                                      :record 6
14                                      :record 7
21                                      :record 8
22                                      :record 9
23                                      :record 10
25                                      :record 11 (1+NDM)
```

Explanation of Records

(1)

NDM: Number of disk modes to be included in forced response calculation.

(2 to 1+NDM)

Mode numbers of disk modes to be included in calculation.

File *blade.in* — Input File for Subprogram *blade*

```
3                                       NBM:record 1
1                                       :record 2
3                                       :record 3
4                                       :record 4 (1+NBM)

2                                       NF:record 5 (1+NBM+1)
8       3       (1.0, 0.0)              :record 6 (1+NBM+2)
9       5       (1.0, 0.0)              :record 7 (1+NBM+1+NF)
```

Explanation of Records

(1)

NBM: Number of blade modes to be included in forced response calculation.

(2 to 1+NBM)

Mode numbers of blade modes to be included in calculation.

(1+NBM+1)

NF: Number of non-zero components of excitation forces to be specified.

(1+NBM+2 to 1+NBM+1+NF)

Non-zero components (in blade coordinates) of excitation forces. In this example, record 6 specifies that force component 3 on blade node 8 is (1.0,0.0) and record 7 specifies that force component 5 on blade node 9 is (1.0,0.0).

Notice that force components have to be specified by complex numbers to take into account the possible phase difference between force components.

File *interface.in* — Input File for Subprogram *interface*

```
6                                       NK:record 1
1       1       (1.00E55, 0.0)          :record 2
2       2       (1.00E55, 0.0)          :record 3
3       3       (1.00E08, 0.0)          :record 4
4       4       (8.70E05, 0.0)          :record 5
5       5       (7.20E08, 0.0)          :record 6
6       6       (1.00E55, 0.0)          :record 7 (1+NK)
```

Explanation of Records

(1)

NK: Number of non-zero components (in blade coordinates) to be specified for the disk-blade attachment stiffness matrix K_{00}. (K_{00} is a 6x6 complex matrix.)

(2 to 1+NK)

Non-zero components of K_{00}. In this example,

record 2: stiffness in x direction is infinite.

record 3: stiffness in y direction is infinite.

record 4: stiffness in z direction is (1.00E08,0.0).

record 5: torsional stiffness in x direction is (8.70E05,0.0).

record 6: torsional stiffness in y direction is (7.20E08,0.0).

record 7: torsional stiffness in z direction is infinite.

Notice that stiffness components have to be specified by complex numbers to take into account the possible damping mechanism.

File *ranbld.in* — Input File for Subprogram *ranbld*

```
3                                       :record 1
1                                       :record 2
3                                       :record 3
50.0                                    :record 4
874377                                  :record 5
```

Explanation of Records

(1)

Indicator for blade natural frequency disturbance.

1 = identical blades.

2 = sinusoidal distribution.

3 = gaussian distribution.

(2)

Blade mode to be disturbed.

(3)

Indicator for the frequency disturbance on other modes.

1 = no disturbance.

2 = same magnitude.

3 = same percentage.

(4)

Amplitude (sinusoidal distribution) or standard deviation (gaussian distribution) of the disturbance in Hz.

(5)

Number of nodal diameters of sinusoidal distribution or seed for the gaussian random number generator.

File *assembly.in* — Input File for Subprogram *assembly*

```
1                                          :record 1

4                                          :record 2
4450.0    4950.0    100                    :record 3

0.0025                                     :record 4
2                                          ND:record 5
13        0.0020                           :record 6
14        0.0015                           :record 7 (5+ND)

0.0027                                     :record 8 (5+ND+1)
2                                          NB:record 9 (5+ND+2)
3         0.0022                           :record 10 (5+ND+3)
4         0.0024                           :record 11 (5+ND+2+NB)
```

Explanation of Records

(1)

Flag for error estimate on LU algorithm.

1 = perform.

0 = do not perform.

(2)

Excitation engine order.

(3)

Excitation frequency bounds (in Hz) and number of the intervals of the calculation. In this example, the lower bound is 4450 Hz, the upper bound is 4950 Hz, and the number of intervals is 100. The forced response will be calculated for every 4 Hz from 4450 Hz to 4950 Hz.

(4)

Damping ratio for disk modes in general.

(5)

ND: Number of disk modes with damping ratios to be particularly specified.

(6 to 5+ND)

Mode numbers and damping ratios of the particular disk modes. In this example, record 6 specifies that the damping ratio for disk mode 13 is 0.0020 and record 7 specifies that the damping ratio for disk mode 14 is 0.0015.

(5+ND+1)

Damping ratio for blade modes in general.

(5+ND+2)

NB: Number of blade modes with damping ratios to be particularly specified.

(5+ND+3 to 5+ND+2+NB)

Mode numbers and damping ratios of the particular blade modes. In this example, record 10 specifies that the damping ratio for blade mode 3 is 0.0022 and record 11 specifies that the damping ratio for blade mode 4 is 0.0024.

File *amplitude.in* — Input File for Subprogram *amplitude*

```
2                                   NN:record 1
4                                   :record 2
8                                   :record 3 (1+NN)

2                                   NC:record 4 (1+NN+1)
3                                   :record 5 (1+NN+2)
5                                   :record 6 (1+NN+1+NC)
```

Explanation of Records

(1)

NN: Number of blade nodes to be printed.

(2 to 1+NN)

Blade nodes to be printed. In this example, amplitudes of nodes 3 and 8 will be printed.

(1+NN+1)

NC: Number of displacement components to be printed for each node specified above.

(1+NN+2 to 1+NN+1+NC)

Displacement components (in blade coordinates) to be printed. In this example, displacement components 3 and 5 will be printed.

EXAMPLE RESULT

After successfully running subprogram *amplitude*, the forced response of the bladed disk is stored in file *lmcc.out.amplitude*. This file has documents in the beginning which explain the format of the data printed. The format is designed to be read by general plotting routines. An example of the file is as follows:

```
# Data printed are:

# (column  1) Excitation frequency [Hz]

# (column  2) Amplitude of component   3 of node   4 of blade   1
# (column  3) Amplitude of component   3 of node   4 of blade   2
# (column  4) Amplitude of component   3 of node   4 of blade   3
# (column  5) Amplitude of component   3 of node   4 of blade   4
# (column  6) Amplitude of component   3 of node   4 of blade   5
# (column  7) Amplitude of component   3 of node   4 of blade   6
# (column  8) Amplitude of component   3 of node   4 of blade   7
# (column  9) Amplitude of component   3 of node   4 of blade   8
# (column 10) Amplitude of component   3 of node   4 of blade   9
# (column 11) Amplitude of component   3 of node   4 of blade  10
# (column 12) Amplitude of component   3 of node   4 of blade  11
# (column 13) Amplitude of component   3 of node   4 of blade  12

# (column 14) Amplitude of component   3 of node   8 of blade   1
# (column 15) Amplitude of component   3 of node   8 of blade   2
# (column 16) Amplitude of component   3 of node   8 of blade   3
# (column 17) Amplitude of component   3 of node   8 of blade   4
# (column 18) Amplitude of component   3 of node   8 of blade   5
# (column 19) Amplitude of component   3 of node   8 of blade   6
# (column 20) Amplitude of component   3 of node   8 of blade   7
# (column 21) Amplitude of component   3 of node   8 of blade   8
# (column 22) Amplitude of component   3 of node   8 of blade   9
# (column 23) Amplitude of component   3 of node   8 of blade  10
# (column 24) Amplitude of component   3 of node   8 of blade  11
# (column 25) Amplitude of component   3 of node   8 of blade  12

# (column 26) Amplitude of component   5 of node   4 of blade   1
# (column 27) Amplitude of component   5 of node   4 of blade   2
# (column 28) Amplitude of component   5 of node   4 of blade   3
# (column 29) Amplitude of component   5 of node   4 of blade   4
# (column 30) Amplitude of component   5 of node   4 of blade   5
# (column 31) Amplitude of component   5 of node   4 of blade   6
# (column 32) Amplitude of component   5 of node   4 of blade   7
# (column 33) Amplitude of component   5 of node   4 of blade   8
# (column 34) Amplitude of component   5 of node   4 of blade   9
# (column 35) Amplitude of component   5 of node   4 of blade  10
# (column 36) Amplitude of component   5 of node   4 of blade  11
# (column 37) Amplitude of component   5 of node   4 of blade  12

# (column 38) Amplitude of component   5 of node   8 of blade   1
# (column 39) Amplitude of component   5 of node   8 of blade   2
# (column 40) Amplitude of component   5 of node   8 of blade   3
# (column 41) Amplitude of component   5 of node   8 of blade   4
# (column 42) Amplitude of component   5 of node   8 of blade   5
# (column 43) Amplitude of component   5 of node   8 of blade   6
# (column 44) Amplitude of component   5 of node   8 of blade   7
# (column 45) Amplitude of component   5 of node   8 of blade   8
# (column 46) Amplitude of component   5 of node   8 of blade   9
# (column 47) Amplitude of component   5 of node   8 of blade  10
# (column 48) Amplitude of component   5 of node   8 of blade  11
# (column 49) Amplitude of component   5 of node   8 of blade  12

..... FORCED RESPONSE DATA .....
```

. . . . . .
. . . . . .

ADDITIONAL CONSIDERATION AND POTENTIAL PROBLEMS

While using EAL as the preprocessor of LMCC, we found that EAL occasionally generates disk modes which are not mutually orthogonal. The problem was that modes of the same number of nodal circles and same number of nodal lines should have the same mode shape except that they are out of phase. EAL sometimes generates this kind of modes with correct mode shapes which are not completely out of phase. This kind of error causes the forced response calculation so that LMCC will give meaningless results. Typically when this error occurs, it is indicated by the fact that LMCC predicts unusually high forced response over part of the frequency range.

Appendix C: Theoretical Manual for LMCC

ABSTRACT

This appendix contains the theory of the reduced order algorithm upon which the Linear Mistuning Computer Code (LMCC) is based. Chapter 1 is the introduction and motivation of this research project. Chapter 2 and Chapter 3 state the theory of the reduced order algorithm. Chapter 4 gives some benchmark test cases and the comparison between the reduced order model and the traditional spring-mass model.

Chapter 1: INTRODUCTION AND MOTIVATION

In the use of turbomachinery in modern aircraft, blades have failed from high cycle fatigue because of excessive vibration. Based on experiments and earlier analytical investigations [1-5], it is realized that, because of the rotational periodicity of its geometry, a bladed disk usually has natural frequencies that are clustered in narrow ranges. When the natural frequencies of a system are close together, slight variations in the system's structural properties can cause large changes in its modes, and, consequently, its dynamic response. The sensitivity of a bladed disk's dynamic response to small variations in the frequencies of the blades is referred to in the literature as the "blade mistuning problem" and has been studied extensively. It is important to understand mistuning since it can result in large blade to blade variations and the high response blades can fail from high cycle fatigue. For modern aircraft, such as a space shuttle, the high vibratory response of bladed disks is of special concern because of the severe operating conditions to which they are subjected.

Every year, a great number of experiments are conducted by industry to ensure that the blades are safely designed. These experiments are generally expensive and time-consuming. In order to reduce the time and cost associated with these experiments, turbine manufacturers replace part of the experiments by numerical simulations. From a modeling point of view, traditional simulations can be classified into several categories. One of them is to directly use finite element methods. The direct finite element approach is straight forward and can

accurately model the characteristics of a structure provided that the structure is represented with enough elements. However, since a structurally accurate finite element model for a typical bladed disk can have more than 1,000,000 degrees of freedom, the associated computational time for deriving the eigenvalues and eigenvectors of a single stage can be as high as 1,000 CPU minutes on a CRAY. If a thorough mistuning analysis using Monte Carlo Simulation is desired, the total CPU time it consumes will be prohibitively high. (For example, 100,000 CPU minutes for a 100 stage simulation.) In addition, the extremely large memory requirements for data storage and the numerical errors associated with numerical instabilities make the direct finite element approach unfeasible.

There have been attempts to develop structurally accurate models for bladed disks. Reference may be made to a feature article by Leissa [10], in which, the progress in modeling blades for vibration analyses is discussed. Many of the attempts to develop structurally accurate models for bladed disks use plate elements to represent the disk and beam elements to represent the blades [3,11-13,21]. While there can be blade configurations for which the beam representation may be adequate, plate, thick shell, and even solid elements are often needed to represent modern, low aspect ratio blades. With recent improvements in finite element methods and computer speed, a whole bladed disk could be modeled accurately but, as previously mentioned, it is recognized that the cost of running these programs would be prohibitively high for use during the design process. This leads to the attempts by researchers to use substructuring techniques in which results from finite element analyses of individual substructures are used to obtain the dynamic behavior of the whole bladed disk [14,15]. There have also been attempts to introduce the cyclic symmetric boundary conditions into finite element codes to model bladed disks so that the system modes can be efficiently solved for and, because of the clustered natural frequencies being separated, the numerical stability is improved [7,16,17].

While finite element models with cyclic symmetric boundary conditions can be easily solved for tuned bladed disks, much of the work that has been done in mistuning utilizes spring-mass models to represent the bladed disk [1,2,4,8,18-21] in order to reduce the number of degrees of freedom and to make the problem computationally more tractable. While they may often provide reasonably accurate predictions of the system's response, the model's parameters, such as the mass and the spring constants, are usually chosen in an ad hoc manner and one must question the ability of such simple models to accurately represent such complex systems. Little work has been published which verifies their accuracy.

The goal of this research is to develop a methodology that will directly take the results from a finite element analysis of a tuned system and construct a computationally efficient mistuned model with a reduced number of degrees of freedom. The intent is that the approach will display the structural accuracy of the finite element model and computational efficiency comparable to a spring-mass model.

Chapter 2: RECEPTANCE METHOD AND REDUCED ORDER MODELING

2.1 Receptance Method

In structural dynamics, one widely used analytical method is to subdivide a complex structure into several substructures, analyze the behavior of the individual substructures, and then use the receptance method [6] to reassemble the structure. Receptance method is based on the observation that, for every substructure, the dynamic response is determined by how the substructure interacts with its environment. If the substructure interacts with its environment only at a limited number of interfaces, it is possible to express the degrees of freedom of the entire substructure in terms of the degrees of freedom of these interfaces. The benefit of this method is that when several substructures interact with each other, we only need to solve for the degrees of freedom of the interfaces. Once the degrees of freedom of these interfaces are determined the response of all substructures and, therefore, the whole structure is known.

To apply the receptance method to a bladed disk, let us consider the disk and all of the blades as two separate substructures. We can then write the receptance equations for the disk and the blades

$$\vec{u}^{\,d} = \mathbf{R}^d \vec{f}^{\,d} \tag{2.1}$$

$$\vec{u}^{\,b} = \mathbf{R}^b \vec{f}^{\,b} \tag{2.2}$$

where $\vec{u}^{\,d}$, $\vec{f}^{\,d}$, and $\mathbf{R}^d$ are the displacement, the external force, the receptance associated with the disk, and $\vec{u}^{\,b}$, $\vec{f}^{\,b}$, and $\mathbf{R}^b$ are the displacement, the external force, and the receptance

associated with the blades. By denoting the group of nodes which do not interact with the other substructure by α, and the group of nodes which are residing at the interfaces by β, we can write equations (2.1) and (2.2) in components,

$$\begin{Bmatrix} \vec{u}^{\,d}_{\alpha} \\ \vec{u}^{\,d}_{\beta} \end{Bmatrix} = \begin{bmatrix} \mathbf{R}^{d}_{\alpha,\alpha} \mathbf{R}^{d}_{\alpha,\beta} \\ \mathbf{R}^{d}_{\beta,\alpha} \mathbf{R}^{d}_{\beta,\beta} \end{bmatrix} \begin{Bmatrix} \vec{f}^{\,d}_{\alpha} \\ \vec{f}^{\,d}_{\beta} \end{Bmatrix} \tag{2.3}$$

$$\begin{Bmatrix} \vec{u}^{\,b}_{\alpha} \\ \vec{u}^{\,b}_{\beta} \end{Bmatrix} = \begin{bmatrix} \mathbf{R}^{b}_{\alpha,\alpha} \mathbf{R}^{b}_{\alpha,\beta} \\ \mathbf{R}^{b}_{\beta,\alpha} \mathbf{R}^{b}_{\beta,\beta} \end{bmatrix} \begin{Bmatrix} \vec{f}^{\,b}_{\alpha} \\ \vec{f}^{\,b}_{\beta} \end{Bmatrix} \tag{2.4}$$

Since, in general, the only external forces on the disk are the interactive forces at the disk-blade interfaces, we assume that

$$\vec{f}^{\,d}_{\alpha} = \vec{0} \tag{2.5}$$

Furthermore, if we assume the excitation forces on the blades are prescribed, then, by requiring the displacements to be continuous and the interactive forces to follow Newton's Interactive Force Law,

$$\vec{u}^{\,d}_{\beta} = \vec{u}^{\,b}_{\beta} \tag{2.6}$$

$$\vec{f}^{\,d}_{\beta} = -\vec{f}^{\,b}_{\beta} \tag{2.7}$$

we can solve for the forces at the interfaces using equations (2.3) and (2.4)

$$\vec{f}^{\,b}_{\beta} = -\left(\mathbf{R}^{b}_{\beta,\beta} + \mathbf{R}^{d}_{\beta,\beta}\right)^{-1} \mathbf{R}^{b}_{\beta,\alpha} \vec{f}^{\,b}_{\alpha} \tag{2.8}$$

and

$$\vec{f}^{\,d}_{\beta} = \left(\mathbf{R}^{b}_{\beta,\beta} + \mathbf{R}^{d}_{\beta,\beta}\right)^{-1} \mathbf{R}^{b}_{\beta,\alpha} \vec{f}^{\,b}_{\alpha} \tag{2.9}$$

Since the only unknowns on the right hand sides of equations (2.3) and (2.4) are $\vec{f}^{\,b}_{\beta}$ and $\vec{f}^{\,d}_{\beta}$, the response of the entire bladed disk is known.

The benefit of using equations (2.8) and (2.9) is that we only need to solve the problem in the subspace-β without the necessity of either calculating the inverse of the dynamic impedance of the whole bladed disk or finding the modes for the entire system. However, finding the receptances for the disk and the blades beforehand still can be computationally intensive. A mathematical expression for the receptances of the disk and the blades are

$$\mathbf{R}^d = \left(\mathbf{K}^d - \Omega^2 \mathbf{M}^d + i\Omega \mathbf{C}^d\right)^{-1} \tag{2.10}$$

$$\mathbf{R}^b = \left(\mathbf{K}^b - \Omega^2 \mathbf{M}^b + i\Omega \mathbf{C}^b\right)^{-1} \tag{2.11}$$

where $\mathbf{K}^d$, $\mathbf{M}^d$, and $\mathbf{C}^d$ are the stiffness, mass, and damping matrices of the disk, and $\mathbf{K}^b$, $\mathbf{M}^b$, and $\mathbf{C}^b$ are the stiffness, mass, and damping matrices of the blades. Ω is the excitation frequency. $\mathbf{R}^b$ is a block-diagonal matrix if there is no structural links between the blades.

An alternative way of calculating these receptances is to use the substructures' modes. That is, by applying standard modal analysis, the receptances can be written in the following form

$$\mathbf{R}^d = \sum_j \frac{\vec{\phi}_j^{\,d} \vec{\phi}_j^{\,d\,T}}{m_j^d \left(\omega_j^{d\,2} - \Omega^2 + 2\, i\Omega\, \omega_j^d \zeta_j^d\right)} \tag{2.12}$$

$$\mathbf{R}^b = \sum_j \frac{\vec{\phi}_j^{\,b} \vec{\phi}_j^{\,b\,T}}{m_j^b \left(\omega_j^{b\,2} - \Omega^2 + 2\, i\Omega\, \omega_j^b \zeta_j^b\right)} \tag{2.13}$$

where $\vec{\phi}_j^{\,d}$, m_j^d, ζ_j^d, and ω_j^d are the mode shape, modal mass, modal damping ratio, and natural frequency of the j-th disk mode, and $\vec{\phi}_j^{\,b}$, m_j^b, ζ_j^b, and ω_j^b are the mode shape, modal mass, modal damping ratio, and natural frequency of the j-th blade mode, respectively. This method is in general better that equations (2.10) and (2.11) since, with the substructures' modes derived in advance, using equations (2.12) and (2.13) to calculate the receptances needs merely algebraic multiplications and additions, whereas equations (2.10) and (2.11) involve the calculation of matrix inverses for every excitation frequency. The other benefit of equations (2.12) and (2.13) is that not all of the substructures' modes are needed in the calculation. Since the modes with natural frequencies close to the excitation frequency will dominate the

response, the other modes can be eliminated from the calculation without a significant loss of accuracy.

However, there are still several shortcomings which prevent us from using the receptance formulation (the combination of equations (2.8), (2.9), (2.12), and (2.13)) to solve our problem:

1. The substructures' modes used in equations (2.12) and (2.13) have to be free at the disk-blade interfaces, or, in other words, they have to be admissible. To satisfy this requirement, it is fine for us to use the disk modes which are clamped at the inner edge and free at the outer edge, but it is undesirable to use the free-free blade modes. Because the blades generally vibrate close to the clamped-free condition, we need a large number of the free-free modes to achieve a good representation of blade vibration. Another more realistic reason for not using free-free blade modes is that most of the analyses done on the blades in the industry, either numerically or experimentally, use cantilever blades. There is much more information available on the clamped-free blades than the free-free blades.

2. In equations (2.8) and (2.9), we need to find the inverse of the matrix $\left(\mathbf{R}^{b}_{\beta,\beta} + \mathbf{R}^{d}_{\beta,\beta}\right)$. This matrix has a dimension of the group-β nodes which is much smaller than the dimension of the whole bladed disk, but, still, there can be too many degrees of freedom to be solved for. Since we do not want to restrict our analysis to use a particular type of blade models, for example, beam-type blade model with single-node contact at the disk-blade interface, we need to modify the receptance method to have the capability to handle multiple-point disk-blade attachments.

2.2 Reduced Order Modeling Based On Rigid Blade Base Assumption

One of the reasons that the direct receptance method is not particularly attractive is that there are still too many degrees of freedom. In this section, we would like to propose a reduced order method which is capable of handling multiple-point disk-blade attachments and, yet, results in a formulation having fewer degrees of freedom.

For a system of substructures having multiple point contact with each other, it is in general not possible to reduce the number of degrees of freedom of its receptance formulation. However, for a bladed disk, the deformation of the disk-blade interfaces is in general not significant in comparison with the deformation of the blades. Therefore, except for the case when the high nodal diameter disk modes strongly participate, each of the blade bases can be reasonably approximated by six degrees of freedom, namely, three translations and three rotations. With this assumption, the number of degrees of freedom of the reduced order formulation will be six times of the number of blades which is much smaller than that of the direct receptance formulation.

Chapter 3: MATHEMATICAL FORMULATIONS

Figure 3.1 shows a schematic of a bladed disk assembly. By subdividing the structure along the dashed line as indicated in the figure, we have two types of substructures, namely, the disk (Figure 3.2) and the blades (Figure 3.3). Observing Figures 3.2 and 3.3, one can see that the vibration of the disk is a function of the interactive forces at the disk-blade interfaces. In addition, the dynamic response of the blades is also determined by these interactive forces provided the external excitation on the airfoils are taken into account. As a result, the vibration of the entire structure can be expressed in terms of the interactive forces.

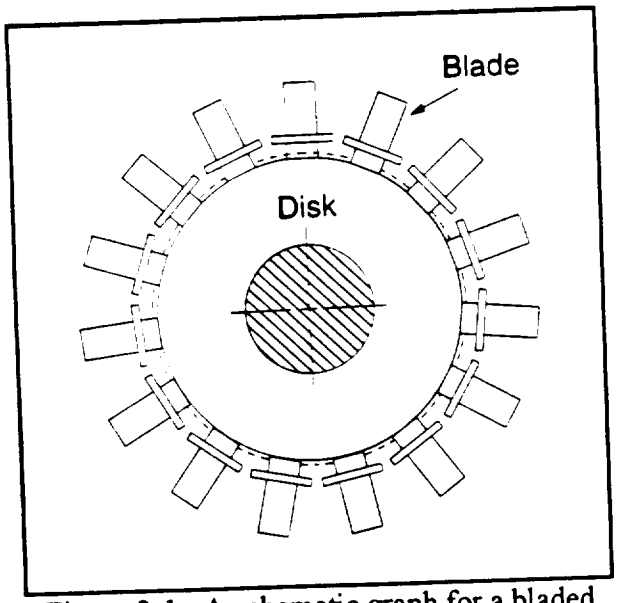

Figure 3-1: A schematic graph for a bladed disk assembly

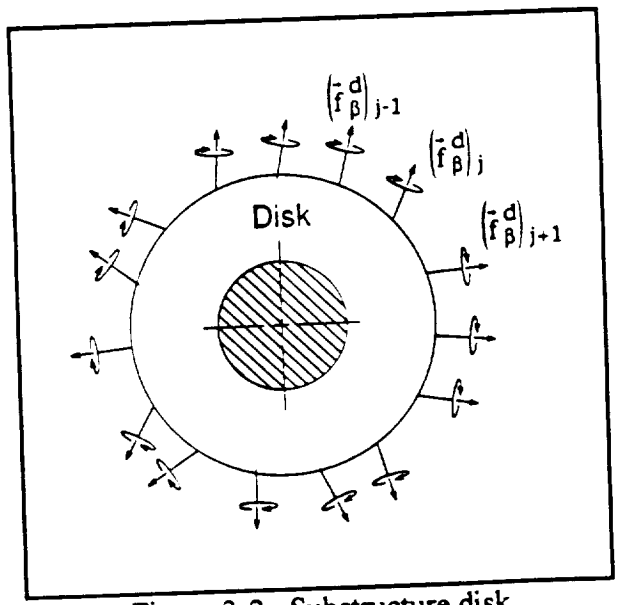

Figure 3-2: Substructure disk

The goal of this chapter is to present the application of the described reduced order approach to bladed disk assemblies. In Sections 3.1 and 3.2, we will present the mathematical formulations which express the vibration of the disk and the blades in terms of the reduced order degrees of freedom of the disk-blade interfaces. In Section 3.3, we will derive the solutions for the whole structure by utilizing the results of Sections 3.1 and 3.2.

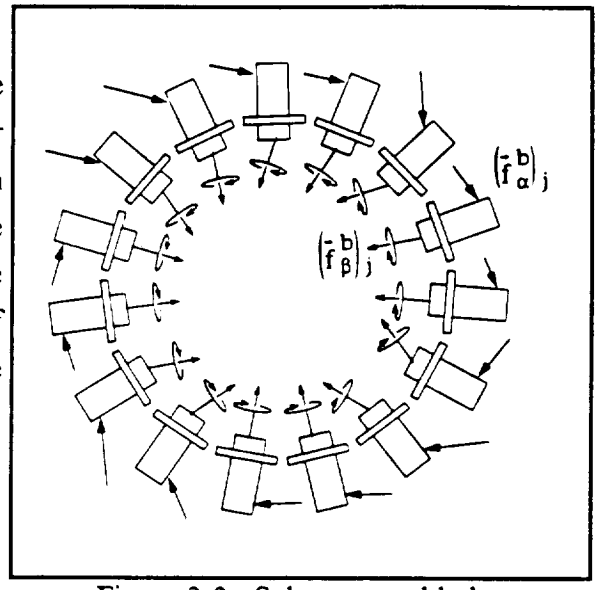

Figure 3-3: Substructure blades

3.1 Formulation for the Disk

3.1.1 Disk receptance

For the disk substructure which is clamped at the inner edge and free at the outer edge, the equation of motion is

$$\mathbf{M}^d \ddot{\vec{x}}^d + \mathbf{C}^d \dot{\vec{x}}^d + \mathbf{K}^d \vec{x}^d = \vec{f}^d e^{i\Omega t} \tag{3.1}$$

where $\mathbf{M}^d$, $\mathbf{C}^d$, and $\mathbf{K}^d$ are the mass, damping, and stiffness matrices respectively, $\vec{x}^d$ is the complex displacement vector whose real part is the physical displacement of the disk, Ω is the excitation frequency, and $\vec{f}^d e^{i\Omega t}$ is the complex forcing vector whose real part is the physical force acting on the disk. When the bladed disk is operated at a stationery speed, the steady-state response of the disk can be written as

$$\vec{x}^d = \vec{u}^d e^{i\Omega t} \tag{3.2}$$

where $\vec{u}^d$ is the complex amplitude vector of the response. By substituting (3.2) into (3.1) and eliminating time dependent terms, we obtain

$$\vec{u}^d = \mathbf{R}^d \vec{f}^d \tag{3.3}$$

where $\mathbf{R}^d$ is the receptance matrix of the disk with the expression

$$\mathbf{R}^d = \left(\mathbf{K}^d - \Omega^2 \mathbf{M}^d + i\Omega \mathbf{C}^d\right)^{-1} \tag{3.4}$$

By applying standard modal analysis technique and approximating the structural damping by modal damping, the disk receptance can be further written as

$$\mathbf{R}^d = \sum_j \frac{\vec{\phi}_j^{\,d} \vec{\phi}_j^{\,d\,T}}{m_j^d \left(\omega_j^{d\,2} - \Omega^2 + 2\, i\Omega\, \omega_j^d \zeta_j^d\right)} \tag{3.5}$$

where $\vec{\phi}_j^{\,d}$ is the j-th disk mode, and m_j^d, ζ_j^d, and ω_j^d are the modal mass, modal damping ratio, and natural frequency of the j-th disk mode, respectively.

To calculate the receptance $\mathbf{R}^d$, equation (3.5) is preferable than equation (3.4) from the computational point of view since equation (3.5) inheres several nice properties:

1. Equation (3.4) involves the calculation of a matrix inverse which is in general computationally expensive. In the case of near or at the natural frequency of the disk, the use of equation (3.4) is particularly undesirable since the dynamic impedance $\left(\mathbf{K}^d - \Omega^2 \mathbf{M}^d + i\Omega \mathbf{C}^d\right)$ tends to be ill-conditioned. On the contrary, equation (3.5) needs merely algebraic multiplications and additions. It is therefore computationally more efficient and reliable.

2. For a particular frequency range of interest, only a limited number of the disk modes dominate the response and the other modes participate in an insignificant manner. By eliminating the insignificant disk modes from the calculation, equation (3.5) still remains an accurate representation of the disk receptance and yet has the advantage of higher computational efficiency. On the other hand, using equation (3.4) to calculate the disk receptance would require an intensive computational effort independent of the frequency range of interest.

3. The disk receptance for the reduced degrees of freedom of the disk interfaces can be easily derived using equation (3.5) and results in a computationally efficient approach. However, using equation (3.4) for the same purpose does not have such a benefit. We will see the reason for this in the next section.

3.1.2 Disk receptance at the disk-blade interfaces

As was mentioned in Chapter 2, the response of the disk is a function of the interactive forces that act between the disk and the blades. To derive the disk receptance associated with the disk-blade interfaces, we need to write the force vector $\vec{f}^{\,d}$ and the mode shape vector $\vec{\phi}_j^{\,d}$ in components,

$$\vec{\phi}_j^{\,d} = \begin{Bmatrix} \vec{\phi}_{j,\alpha}^{\,d} \\ \vec{\phi}_{j,\beta}^{\,d} \end{Bmatrix} \tag{3.6}$$

$$\vec{f}^{\,d} = \begin{Bmatrix} \vec{f}_{\alpha}^{\,d} \\ \vec{f}_{\beta}^{\,d} \end{Bmatrix} \tag{3.7}$$

where the subscript "β" indicates the disk-blade interfaces and "α" indicates the other parts of the disk. Since the only forces acting on the disk are the interactive forces between the disk and the blades, we have

$$\vec{f}_{\alpha}^{\,d} = \vec{0} \tag{3.8}$$

Combining equations (3.3), (3.5), (3.6), (3.7), and (3.8) we obtain

$$\vec{u}^{\,d} = \sum_j \frac{\vec{\phi}_j^{\,d}\, \vec{\phi}_{j,\beta}^{\,d\,T}}{m_j^d \left(\omega_j^{d\,2} - \Omega^2 + 2\, i\, \Omega\, \omega_j^d\, \zeta_j^d\right)} \vec{f}_{\beta}^{\,d} \tag{3.9}$$

In particular, if we are interested in the displacement of the interfaces, equation (3.9) implies

$$\vec{u}_{\beta}^{\,d} = \mathbf{R}_{\beta,\beta}^{d}\, \vec{f}_{\beta}^{\,d} \tag{3.10}$$

where $\vec{u}_{\beta}^{\,d}$ is the displacement of the disk at the interfaces. $\mathbf{R}_{\beta,\beta}^{d}$ is the disk receptance associated with the interfaces and is given by,

$$\mathbf{R}^{d}_{\beta,\beta} = \sum_{j} \frac{\vec{\phi}^{d}_{j,\beta}\,\vec{\phi}^{d\,T}_{j,\beta}}{m^{d}_{j}\left(\omega^{d\,2}_{j} - \Omega^{2} + 2\,i\,\Omega\,\omega^{d}_{j}\,\zeta^{d}_{j}\right)} \tag{3.11}$$

The key results of this section is the reduced disk receptance equation (3.10) which governs the relation between the forces and the displacements of the nodes associated with the disk interface degrees of freedom.

3.1.3 Deriving six equivalent degrees of freedom for each disk-blade interface

It was discussed in Chapter 2 that the disk receptance associated with the interfaces still has too many degrees of freedom to be optimally efficient. The goal of this section is to derive a reduced ordered disk receptance which has significantly fewer degrees of freedom. The basic idea is to find six equivalent degrees of freedom which will approximately represent the disk at each disk-blade interface. Assume that, for the j-th disk interface, the translation and rotation about a reference point O is approximately given by $\vec{v}^{d}_{o}$ and $\vec{\theta}^{d}_{o}$ respectively. (Here, we omit the subscript "j" temporarily for the simplicity of writing.) If we denote the translation of the k-th disk node of this interface as $\vec{v}^{d}_{k}$ and the rotation of the node as $\vec{\theta}^{d}_{k}$, then, for small amplitude vibration, we can write

$$\vec{v}^{d}_{k} \approx \vec{v}^{d}_{o} + \vec{\theta}^{d}_{o} \times \vec{\rho}^{d}_{k} \tag{3.12}$$

$$\vec{\theta}^{d}_{k} \approx \vec{\theta}^{d}_{o} \tag{3.13}$$

where $\vec{\rho}^{d}_{k}$ is the position vector from point O to the k-th node. If we define the vectors

$$\vec{u}^{d}_{o} = \begin{Bmatrix} \vec{v}^{d}_{o} \\ \vec{\theta}^{d}_{o} \end{Bmatrix} \tag{3.14}$$

$$\vec{u}^{d}_{k} = \begin{Bmatrix} \vec{v}^{d}_{k} \\ \vec{\theta}^{d}_{k} \end{Bmatrix} \tag{3.15}$$

k = 1, 2, ..., DNI, where DNI is the number of disk nodes at the disk-blade interface, then equations (3.12) and (3.13) can be cast in matrix form

$$\vec{u}^{\,d}_{k} \approx \mathbf{Q}^{d}_{k,o}\,\vec{u}^{\,d}_{o} \tag{3.16}$$

where

$$\mathbf{Q}^{d}_{k,o} = \begin{bmatrix} \mathbf{I} & \mathbf{W}^{d}_{k,o} \\ 0 & \mathbf{I} \end{bmatrix} \tag{3.17}$$

$$\mathbf{W}^{d}_{k,o} = \begin{bmatrix} 0 & \left(\vec{\rho}^{\,d}_{k}\right)_z & -\left(\vec{\rho}^{\,d}_{k}\right)_y \\ -\left(\vec{\rho}^{\,d}_{k}\right)_z & 0 & \left(\vec{\rho}^{\,d}_{k}\right)_x \\ \left(\vec{\rho}^{\,d}_{k}\right)_y & -\left(\vec{\rho}^{\,d}_{k}\right)_x & 0 \end{bmatrix} \tag{3.18}$$

and $\mathbf{I}$ is the 3 by 3 identity matrix.

Now, since $\vec{u}^{\,d}_{\beta}$ is the displacement vector for all of the disk nodes at the disk-blade interface, we have

$$\vec{u}^{\,d\,T}_{\beta} = \left[\vec{u}^{\,d\,T}_{1} \;\ldots \vec{u}^{\,d\,T}_{k} \;\ldots \vec{u}^{\,d\,T}_{DNI}\right] \tag{3.19}$$

Then equations (3.16) and (3.19) imply

$$\vec{u}^{\,d}_{\beta} \approx \mathbf{Q}^{d}_{\beta,o}\,\vec{u}^{\,d}_{o} \tag{3.20}$$

where

$$\mathbf{Q}^{d\,T}_{\beta,o} = \left[\mathbf{Q}^{d\,T}_{1,o} \ldots \mathbf{Q}^{d\,T}_{k,o} \ldots \mathbf{Q}^{d\,T}_{DNI,o}\right] \tag{3.21}$$

Without dropping the subscript "j" for the j-th disk-blade interface, equation (3.20) would be written as

$$\left(\vec{u}^{\,d}_{\beta}\right)_j \approx \left(\mathbf{Q}^{d}_{\beta,o}\right)_j \left(\vec{u}^{\,d}_{o}\right)_j \tag{3.22}$$

Then, for all of the interfaces, equation (3.22) implies

$$\vec{u}^{\,d}_{\beta} \approx Q^{d}_{\beta,o}\,\vec{u}^{\,d}_{o} \tag{3.23}$$

where, with the number of blades being denoted by NB,

$$\vec{u}^{\,d\,T}_{\beta} = \left[\left(\vec{u}^{\,d}_{\beta}\right)^{T}_{1} \ldots \left(\vec{u}^{\,d}_{\beta}\right)^{T}_{k} \ldots \left(\vec{u}^{\,d}_{\beta}\right)^{T}_{NB}\right] \tag{3.24}$$

$$Q^{d}_{\beta,o} = \mathrm{diag}\left[\left(Q^{d}_{\beta,o}\right)_{1} \ldots \left(Q^{d}_{\beta,o}\right)_{k} \ldots \left(Q^{d}_{\beta,o}\right)_{NB}\right] \tag{3.25}$$

$$\vec{u}^{\,d\,T}_{o} = \left[\left(\vec{u}^{\,d}_{o}\right)^{T}_{1} \ldots \left(\vec{u}^{\,d}_{o}\right)^{T}_{k} \ldots \left(\vec{u}^{\,d}_{o}\right)^{T}_{NB}\right] \tag{3.26}$$

Notice here that $Q^{d}_{\beta,o}$ is a block-diagonal matrix with diagonal blocks $\left(Q^{d}_{\beta,o}\right)_{k}$ (k = 1, ..., NB)$_d$. Equation (3.23) gives an approximate relation between the reduced order displacements $\vec{u}^{\,d}_{o}$ and the displacements of the interfacial disk nodes $\vec{u}^{\,d}_{\beta}$. $\vec{u}^{\,d}_{o}$ is a vector with dimension 6•NB and $\vec{u}^{\,d}_{\beta}$ has a dimension of 6•DNI•NB. $Q^{d}_{\beta,o}$ is a rectangular matrix with dimension 6•DNI•NB by 6•NB.

We also need to find the resultant forces and moments for the each interface. For the j-th disk interface, the resultant force and moment about the reference point O are

$$\vec{\pi}^{\,d}_{o} = \sum_{k} \vec{\pi}^{\,d}_{k} \tag{3.27}$$

$$\vec{\tau}^{\,d}_{o} = \sum_{k} \vec{\tau}^{\,d}_{k} + \vec{\rho}^{\,d}_{k} \times \vec{\pi}^{\,d}_{k} \tag{3.28}$$

where $\vec{\pi}^{\,d}_{o}$ is the resultant force acting on the disk at the disk interface and $\vec{\tau}^{\,d}_{o}$ is the resultant moment about the reference point O acting on the disk at the interface. $\vec{\pi}^{\,d}_{k}$ is the force acting on the k-th disk node of the j-th interface and $\vec{\tau}^{\,d}_{k}$ is the moment acting on the k-the disk node of the j-th interface. Notice here that the subscript "j" is temporarily omitted for simplicity in writing. Equations (3.27) and (3.28) can be rewritten in matrix form by using the procedure presented earlier,

$$\begin{Bmatrix} \vec{\pi}^{\,d}_{o} \\ \vec{\tau}^{\,d}_{o} \end{Bmatrix} = \sum_{k} \begin{bmatrix} \mathbf{I} & 0 \\ \mathbf{W}^{d\,T}_{k,o} & \mathbf{I} \end{bmatrix} \begin{Bmatrix} \vec{\pi}^{\,d}_{k} \\ \vec{\tau}^{\,d}_{k} \end{Bmatrix} \tag{3.29}$$

where the skew-symmetric matrix $\mathbf{W}^{d}_{k,o}$ has been defined in equation (3.18). If we define the vector

$$\vec{f}^{\,d}_{o} = \begin{Bmatrix} \vec{\pi}^{\,d}_{o} \\ \vec{\tau}^{\,d}_{o} \end{Bmatrix} \tag{3.30}$$

and recognize that

$$\vec{f}^{\,d\,T}_{\beta} = \begin{bmatrix} \vec{\pi}^{\,d\,T}_{1} & \vec{\tau}^{\,d\,T}_{1} & \ldots \vec{\pi}^{\,d\,T}_{k} & \vec{\tau}^{\,d\,T}_{k} & \ldots \vec{\pi}^{\,d\,T}_{DNI} & \vec{\tau}^{\,d\,T}_{DNI} \end{bmatrix} \tag{3.31}$$

then equation (3.30) can be written as

$$\vec{f}^{\,d}_{o} = \mathbf{Q}^{d\,T}_{\beta,o}\, \vec{f}^{\,d}_{\beta} \tag{3.33}$$

where $\mathbf{Q}^{d}_{\beta,c}$ has been previously defined in equation (3.21). Now, using the subscript "j" which was dropped previously, equation (3.33) would be in fact written as

$$\left(\vec{f}^{\,d}_{o}\right)_{j} = \left(\mathbf{Q}^{d}_{\beta,o}\right)^{T}_{j} \left(\vec{f}^{\,d}_{\beta}\right)_{j} \tag{3.34}$$

Therefore, for all of the disk-blade interfaces, equation (3.34) implies

$$\vec{f}^{\,d}_{o} = \mathbf{Q}^{d\,T}_{\beta,o}\, \vec{f}^{\,d}_{\beta} \tag{3.35}$$

where, with NB denoting the number of blades,

$$\vec{f}^{\,d\,T}_{o} = \left[\left(\vec{f}^{\,d}_{o}\right)^{T}_{1} \ldots \left(\vec{f}^{\,d}_{o}\right)^{T}_{k} \ldots \left(\vec{f}^{\,d}_{o}\right)^{T}_{NB} \right] \tag{3.36}$$

$$\vec{f}^{\,d\,T}_{\beta} = \left[\left(\vec{f}^{\,d}_{\beta}\right)^{T}_{1} \ldots \left(\vec{f}^{\,d}_{\beta}\right)^{T}_{k} \ldots \left(\vec{f}^{\,d}_{\beta}\right)^{T}_{NB} \right] \tag{3.37}$$

and $\mathbf{Q}^{d}_{\beta,o}$ was defined in equation (3.25). Equation (3.35) governs the relation between the resultant interfacial forces, $\vec{f}^{\,d}_{o}$, and the individual nodal forces, $\vec{f}^{\,d}_{\beta}$, of the interfacial nodes for every disk interface. $\vec{f}^{\,d}_{o}$ and $\vec{f}^{\,d}_{\beta}$ are vectors with dimensions 6•NB and 6•DNI•NB respectively.

3.1.4 Reduced order disk receptance

Equation (3.10) governs the relation between the actual interactive forces and the actual displacements of the disk nodes at the interfaces. Equations (3.23) and (3.35) describe the relation between actual degrees of freedom and the reduced order ones. To find the relation between the reduced order forces $\vec{f}^{\,d}_{o}$ and the reduced order displacements $\vec{u}^{\,d}_{o}$, we need to find the inverse functions for equation (3.23) and (3.35). For equation $(3.23)_d$ since $\vec{u}^{\,d}_{o}$ is overdetermined by $\vec{u}^{\,d}_{\beta}$, it is possible to find a least square approximation of $\vec{u}^{\,d}_{o}$ such that the error

$$\text{Error} = \left|\left| \vec{u}^{\,d}_{\beta} - Q^{d}_{\beta,o}\, \vec{u}^{\,d}_{o} \right|\right|^2 \tag{3.38}$$

is minimized. The least square approximation of $\vec{u}^{\,d}_{o}$ can be mathematically written in a simple form

$$\vec{u}^{\,d}_{o} = Q^{d}_{\beta,o}{}^{+}\, \vec{u}^{\,d}_{\beta} \tag{3.39}$$

where $Q^{d}_{\beta,o}{}^{+}$ is the generalized inverse of $Q^{d}_{\beta,c}$ with the expression

$$Q^{d}_{\beta,o}{}^{+} = \left(Q^{d}_{\beta,o}{}^{T}\, Q^{d}_{\beta,o}\right)^{-1} Q^{d}_{\beta,o}{}^{T} \tag{3.40}$$

For equation (3.35), since $\vec{f}^{\,d}_{\beta}$ is under-determined by $\vec{f}^{\,d}_{o}$, there are many possible approximations of $\vec{f}^{\,d}_{\beta}$ for every given $\vec{f}^{\,d}_{o}$. However, by requesting that the norm of $\vec{f}^{\,d}_{\beta}$ to be minimized, it is possible for us to find a unique approximation of $\vec{f}^{\,d}_{\beta}$ that retains the non-self-equilibrated forces only and neglects the self-equilibrated forces. The expression for the non-self-equilibrated approximation is

$$\vec{f}^{\,d}_{\beta} = \left(Q^{d}_{\beta,o}{}^{+}\right)^{T} \vec{f}^{\,d}_{o} \tag{3.41}$$

where $Q^{d}_{\beta,o}{}^{+}$ is defined in equation (3.40).

Here we are actually proposing an assumption that the self-equilibrated forces at the interfaces are negligible. This assumption should be valid for the lower system modes since the disk does not locally deform very much in these cases. It, however, may not be

Combining equations (3.10), (3.39), and (3.41), we can have the following equation

$$\vec{u}^{\,d}_{o} = \mathbf{R}^{d}_{o,o}\,\vec{f}^{\,d}_{o} \tag{3.42}$$

where

$$\mathbf{R}^{d}_{o,o} = \sum_{j} \frac{\vec{\phi}^{\,d}_{j,o}\,\vec{\phi}^{\,d\,T}_{j,o}}{m^{d}_{j}\left(\omega^{d\,2}_{j} - \Omega^{2} + 2\,i\,\Omega\,\omega^{d}_{j}\,\zeta^{d}_{j}\right)} \tag{3.43}$$

and

$$\vec{\phi}^{\,d}_{j,o} = \mathbf{Q}^{d}_{\beta,o}\,\vec{\phi}^{\,+\,d}_{j,\beta} \tag{3.44}$$

$\mathbf{R}^{d}_{o,o}$ is the reduced order disk receptance matrix associated with the disk interfaces and has dimension 6•NB by 6•NB. $\vec{\phi}^{\,d}_{j,o}$ is the reduced order interfacial displacements for the j-th disk mode. Equation (3.42) is the reduced order disk receptance equation which governs the relation between the reduced order displacements $\vec{u}^{\,d}_{o}$ and the reduced order forces $\vec{f}^{\,d}_{o}$. Remember that this equation is the reduced order form of equation (3.10), the disk receptance equation associated with the disk-blade interfaces. Based on the assumption that the self-equilibrated forces at the interfaces are negligible, equation (3.42) approximates the disk behavior by 6 degrees of freedom per interface.

3.2 Formulation for the Blades

3.2.1 Receptance formulation for a single blade

To begin with, let us consider a single blade which is clamped at its base. The blade base moves rigidly so that its motion can be fully described by 6 degrees of freedom, namely, 3 translations and 3 rotations. Let $\vec{x}^{\,b}_{o}$ be the 6-degree-of-freedom displacement vector of the blade base, where O is a reference point residing at the blade base. Using subscript "β" to denote the group of blade nodes which reside at the blade base and subscript "α" to denote the nodes other than the nodes of group β, the equations of motion for the entire blade can be written as

$$\mathbf{M}^{b}_{\alpha,\alpha}\,\ddot{\vec{z}}^{b}_{\alpha} + \mathbf{C}^{b}_{\alpha,\alpha}\,\dot{\vec{z}}^{b}_{\alpha} + \mathbf{K}^{b}_{\alpha,\alpha}\,\vec{z}^{b}_{\alpha} = \vec{f}^{b}_{\alpha}\, e^{i\Omega t} - \mathbf{M}^{b}_{\alpha,\alpha}\,\mathbf{Q}^{b}_{\alpha,o}\,\ddot{\vec{x}}^{b}_{o} \tag{3.45}$$

$$\vec{x}^{b}_{\alpha} = \vec{z}^{b}_{\alpha} + \mathbf{Q}^{b}_{\alpha,o}\,\vec{x}^{b}_{o} \tag{3.46}$$

$$\vec{x}^{b}_{\beta} = \mathbf{Q}^{b}_{\beta,o}\,\vec{x}^{b}_{o} \tag{3.47}$$

where $\mathbf{M}^{b}_{\alpha,\alpha}$, $\mathbf{C}^{b}_{\alpha,\alpha}$, and $\mathbf{K}^{b}_{\alpha,\alpha}$ are the mass, damping, and stiffness matrices associated with the group-α nodes. $\vec{x}^{b}_{\alpha}$ and $\vec{x}^{b}_{\beta}$ are the displacements of the blade. $\mathbf{Q}^{b}_{\alpha,o}\,\vec{x}^{b}_{o}$ is the displacement vector of the group-α nodes assuming that the blade follows the base and does not deform at all. $\vec{z}^{b}_{\alpha}$ is the deformation of the group-α nodes relative to the undeformed configuration. $\vec{f}^{b}_{\alpha}\, e^{i\Omega t}$ is the external force acting on the blade. $\mathbf{M}^{b}_{\alpha,\alpha}\,\mathbf{Q}^{b}_{\alpha,o}\,\ddot{\vec{x}}^{b}_{o}$ is an inertial force associated with the blade base motion that is introduced when writing the equations of motion in terms of relative motion. The derivations of matrices $\mathbf{Q}^{b}_{\alpha,o}$ and $\mathbf{Q}^{b}_{\beta,o}$ are similar to the process described in Section 3.1.3; we will not repeat it here. When the bladed disk is operated at a stationery speed, the steady-state response of the blade can be written as

$$\vec{x}^{b}_{\alpha} = \vec{u}^{b}_{\alpha}\, e^{i\Omega t} \tag{3.48}$$

$$\vec{x}^{b}_{\beta} = \vec{u}^{b}_{\beta}\, e^{i\Omega t} \tag{3.49}$$

$$\vec{x}^{b}_{o} = \vec{u}^{b}_{o}\, e^{i\Omega t} \tag{3.50}$$

Substituting equations (3.48), (3.49), and (3.50) back into equations (3.45), (3.46), and (3.47) and eliminating time-dependent terms, we have

$$\vec{u}^{b}_{\alpha} = \mathbf{R}^{b}_{\alpha,\alpha}\,\vec{f}^{b}_{\alpha} + \left(\Omega^{2}\,\mathbf{R}^{b}_{\alpha,\alpha}\,\mathbf{M}^{b}_{\alpha,\alpha} + \mathbf{I}\right)\mathbf{Q}^{b}_{\alpha,o}\,\vec{u}^{b}_{o} \tag{3.51}$$

$$\vec{u}^{b}_{\beta} = \mathbf{Q}^{b}_{\beta,o}\,\vec{u}^{b}_{o} \tag{3.52}$$

where $\mathbf{R}^{b}_{\alpha,\alpha}$ is the receptance matrix associated with the group-α nodes. It has the expression

$$\mathbf{R}^{b}_{\alpha,\alpha} = \left(\mathbf{K}^{b}_{\alpha,\alpha} - \Omega^2\,\mathbf{M}^{b}_{\alpha,\alpha} + i\,\Omega\,\mathbf{C}^{b}_{\alpha,\alpha}\right)^{-1} \tag{3.53}$$

As discussed in Section 3.1.1, calculating the inverse of the dynamic impedance matrix $\left(\mathbf{K}^{b}_{\alpha,\alpha} - \Omega^2\,\mathbf{M}^{b}_{\alpha,\alpha} + i\,\Omega\,\mathbf{C}^{b}_{\alpha,\alpha}\right)$ is undesirable since the matrix tends to be ill-conditioned when the excitation frequency Ω is close to the natural frequencies of the blade. Similar to the way we formulate the receptance equation for the disk, the receptance $\mathbf{R}^{b}_{\alpha,\alpha}$ can be cast in the following form by applying the standard modal analysis technique,

$$\mathbf{R}^{b}_{\alpha,\alpha} = \sum_{j} \frac{\vec{\phi}^{\,b}_{j,\alpha}\,\vec{\phi}^{\,b\,T}_{j,\alpha}}{m^{b}_{j}\left(\omega^{b\,2}_{j} - \Omega^2 + 2\,i\,\Omega\,\omega^{b}_{j}\,\zeta^{b}_{j}\right)} \tag{3.54}$$

where $\vec{\phi}^{\,b}_{j,\alpha}$ is the j-th mode for a blade clamped at its base, and m^{b}_{j}, ζ^{b}_{j}, and ω^{b}_{j} are the modal mass, modal damping ratio, and natural frequency of the j-th mode. It should be emphasized that the degrees of freedom of the group-β nodes do not appear in equation (3.54) since $\vec{\phi}^{\,b}_{j,\beta}$, the mode shapes at the blade's base, are zero.

3.2.2 Force on the blade base

While equations (3.51) and (3.52) enable us to calculate the motion of the blade for any given external excitation $\vec{f}^{\,b}_{\alpha}$ and blade base motion $\vec{u}^{\,b}_{o}$, we have not yet determined the resultant force on the blade base. The resultant force on the blade base, denoted as $\vec{f}^{\,b}_{o}$ hereafter, needs to be known in order to assemble the equations for the disk-blade interfaces. To achieve this, we first consider the blade as an object which can move and deform in space. The forces acting on the blade are the excitation force $\vec{f}^{\,b}_{\alpha}$ and the interactive force at the blade interface $\vec{f}^{\,b}_{o}$. Since the linear momentum and angular momentum have to be conserved, we can write the conservation law, about the reference point O, for small amplitude vibrations,

$$\sum_{k} \vec{\dot{L}}^{\,b}_{k} = \sum_{k} \vec{\pi}^{\,b}_{k}\, e^{i\Omega t} \tag{3.55}$$

$$\sum_{k} \vec{\dot{H}}^{\,b}_{k} + \vec{\rho}^{\,b}_{k} \times \vec{\dot{L}}^{\,b}_{k} = \sum_{k} \left(\vec{\tau}^{\,b}_{k} + \vec{\rho}^{\,b}_{k} \times \vec{\pi}^{\,b}_{k}\right) e^{i\Omega t} \tag{3.56}$$

where $\vec{L}^{\,b}_{k}$ is the linear momentum of the k-th blade node, $\vec{H}^{\,b}_{k}$ is the angular momentum of the k-th node about the node itself, $\vec{\pi}^{\,b}_{k}$ and $\vec{\tau}^{\,b}_{k}$ are the force and the moment acting on the k-th

blade node, and $\vec{\rho}_k^{\,b}$ is the position vector from the reference point O to the k-th node. By defining the following 2 vectors,

$$\vec{p}^{\,T} = \begin{bmatrix} \vec{L}_1^{\,bT} & \vec{H}_1^{\,bT} & \cdots & \vec{L}_k^{\,bT} & \vec{H}_k^{\,bT} & \cdots & \vec{L}_{BN}^{\,bT} & \vec{H}_{BN}^{\,bT} \end{bmatrix} \tag{3.57}$$

$$\vec{f}^{\,T} = \begin{bmatrix} \vec{\pi}_1^{\,bT} & \vec{\tau}_1^{\,bT} & \cdots & \vec{\pi}_k^{\,bT} & \vec{\tau}_k^{\,bT} & \cdots & \vec{\pi}_{BN}^{\,bT} & \vec{\tau}_{BN}^{\,bT} \end{bmatrix} \tag{3.58}$$

where BN is the number of blade nodes, equations (3.55) and (3.56) can be rewritten in matrix form,

$$\mathbf{Q}_o^{bT}\,\dot{\vec{p}}^{\,b} = \mathbf{Q}_o^{bT}\,\vec{f}^{\,b}\,e^{i\Omega t} \tag{3.59}$$

where $\mathbf{Q}_o^b$ is a 6•BN by 6 matrix which can be derived by the same procedure presented in Section 3.1. $\mathbf{Q}_o^{bT}$ has the function of calculating the resultant momentum about the reference point O.

Now, by definition, the momentum of the blade can be written as

$$\vec{p}^{\,b} = \mathbf{M}^b\,\dot{\vec{x}}^{\,b} \tag{3.60}$$

where $\mathbf{M}^b$ is the mass matrix of the entire blade. For the steady-state vibration,

$$\vec{x}^{\,b} = \vec{u}^{\,b}\,e^{i\Omega t} \tag{3.61}$$

Substituting equations (3.60) and (3.61) into equation (3.59) and eliminating the time-dependent terms, we have

$$-\Omega^2\,\mathbf{Q}_o^{bT}\,\mathbf{M}^b\,\vec{u}^{\,b} = \mathbf{Q}_o^{bT}\,\vec{f}^{\,b} \tag{3.62}$$

Recall that equations (3.51) and (3.52) describe the displacements of the blade nodes. By substituting them into equation (3.62) and recognizing that

$$\vec{f}_o^{\,b} = \mathbf{Q}_{\beta,o}^{bT}\,\vec{f}_\beta^{\,b} \tag{3.63}$$

we have

$$\vec{f}^{\,b}_{o} = \mathbf{Z}^{b}_{o,o}\,\vec{u}^{\,b}_{o} + \mathbf{H}^{b}_{o,\alpha}\,\vec{f}^{\,b}_{\alpha} \tag{3.64}$$

where

$$\mathbf{Z}^{b}_{o,o} = -\Omega^2\,\mathbf{Q}^{b\,T}_{o}\,\mathbf{M}^{b}\,\mathbf{Q}^{b}_{o} - \Omega^4\,\mathbf{Q}^{b\,T}_{\alpha,o}\,\mathbf{M}^{b}_{\alpha,\alpha}\,\mathbf{R}^{b}_{\alpha,\alpha}\,\mathbf{M}^{b}_{\alpha,\alpha}\,\mathbf{Q}^{b}_{\alpha,o} \tag{3.65}$$

$$\mathbf{H}^{b}_{o,\alpha} = -\Omega^2\,\mathbf{Q}^{b\,T}_{\alpha,o}\,\mathbf{M}^{b}_{\alpha,\alpha}\,\mathbf{R}^{b}_{\alpha,\alpha} - \mathbf{Q}^{b\,T}_{\alpha,o} \tag{3.66}$$

Equation (3.64) gives the expression of $\vec{f}^{\,b}_{o}$, the interactive force acting on the blade base, in terms of the blade base displacement $\vec{u}^{\,b}_{o}$ and the external excitation $\vec{f}^{\,b}_{\alpha}$. The calculation of the coefficient matrices $\mathbf{Z}^{b}_{o,c}$ and $\mathbf{H}^{b}_{o,\alpha}$ are tedious but straight forward. Notice again that the blade receptance $\mathbf{R}^{b}_{\alpha,\alpha}$ will be calculated using the blade modes (equation (3.54)) instead of directly finding the inverse of the dynamic impedance (equation (3.53)). This remark is important since equation (3.54) is efficient and stable when implemented computationally.

3.2.3 Formulation for all blades

Equation (3.64) is written for the j-th blade. Including the subscript "j", it should be written as

$$\left(\vec{f}^{\,b}_{o}\right)_j = \left(\mathbf{Z}^{b}_{o,o}\right)_j \left(\vec{u}^{\,b}_{o}\right)_j + \left(\mathbf{H}^{b}_{o,\alpha}\right)_j \left(\vec{f}^{\,b}_{\alpha}\right)_j \tag{3.66}$$

Therefore, for all of the blades, the equation that governs the states of the blade bases is

$$\vec{f}^{\,b}_{o} = \mathbf{Z}^{b}_{o,o}\,\vec{u}^{\,b}_{o} + \mathbf{H}^{b}_{o,\alpha}\,\vec{f}^{\,b}_{\alpha} \tag{3.67}$$

where

$$\vec{f}^{\,b\,T}_{o} = \left[\left(\vec{f}^{\,b}_{o}\right)^{T}_{1} \cdots \left(\vec{f}^{\,b}_{o}\right)^{T}_{j} \cdots \left(\vec{f}^{\,b}_{o}\right)^{T}_{NB}\right] \tag{3.68}$$

$$\vec{u}^{\,b\,T}_{o} = \left[\left(\vec{u}^{\,b}_{o}\right)^{T}_{1} \cdots \left(\vec{u}^{\,b}_{o}\right)^{T}_{j} \cdots \left(\vec{u}^{\,b}_{o}\right)^{T}_{NB}\right] \tag{3.69}$$

$$\vec{f}^{\,b\,T}_{\alpha} = \left[\left(\vec{f}^{\,b}_{\alpha}\right)^{T}_{1} \cdots \left(\vec{f}^{\,b}_{\alpha}\right)^{T}_{j} \cdots \left(\vec{f}^{\,b}_{\alpha}\right)^{T}_{NB}\right] \tag{3.70}$$

$$\mathbf{Z}^{b}_{o,o} = \text{diag}\left[\left(\mathbf{Z}^{b}_{o,o}\right)_1 \cdots \left(\mathbf{Z}^{b}_{o,o}\right)_j \cdots \left(\mathbf{Z}^{b}_{o,o}\right)_{NB}\right] \tag{3.71}$$

$$\mathbf{H}^{b}_{o,\alpha} = \text{diag}\left[\left(\mathbf{H}^{b}_{o,\alpha}\right)_1 \cdots \left(\mathbf{H}^{b}_{o,\alpha}\right)_j \cdots \left(\mathbf{H}^{b}_{o,\alpha}\right)_{NB}\right] \tag{3.72}$$

Notice that $\mathbf{Z}^{b}_{o,c}$ and $\mathbf{H}^{b}_{o,\alpha}$ are block-diagonal matrices with diagonal blocks $\left(\mathbf{Z}^{b}_{o,o}\right)_j$ and $\left(\mathbf{H}^{b}_{o,\alpha}\right)_j$, j = 1, 2, ..., NB, respectively.

3.3 Assembling Disk and Blades

Recall that the purpose of the analysis is to develop a computationally efficient algorithm to solve for the steady-state vibration of the blades. Equations (3.51) and (3.52) enable us to calculate the blade vibration provided that the external excitation $\vec{f}^{\,b}_{\alpha}$ and the blade base motion $\vec{u}^{\,b}_{o}$ are given. Since the external excitation is usually given, our goal is to solve for the blade base motions.

While equation (3.42) governs the motion of the disk nodes residing at the disk-blade interfaces, equation (3.67) governs the motion of the blade nodes residing at the disk-blade interfaces. Since there are 4 unknown vectors, namely, $\vec{u}^{\,d}_{o}$, $\vec{f}^{\,d}_{o}$, $\vec{u}^{\,b}_{o}$, and $\vec{f}^{\,b}_{o}$ in the equations. We need to introduce two additional equations to govern the behavior of the disk-blade interfaces. The first of these is Newton's Interactive Force Law which conserves momentum at the interfaces,

$$\vec{f}^{\,d}_{o} = -\vec{f}^{\,b}_{o} \tag{3.73}$$

The second is Hooke's Law which provides a constitutive relation at the interfaces,

$$\vec{f}^{\,b}_{o} = \mathbf{K}_{o,o}\left(\vec{u}^{\,d}_{o} - \vec{u}^{\,b}_{o}\right) \tag{3.74}$$

where $\mathbf{K}_{o,c}$ is a matrix which represents the stiffness of the disk-blade attachments. Since the attachment stiffness is in general determined by separate analyses, we will consider it as a known quantity. By solving equations (3.42), (3.67), (3.73), and (3.74) simultaneously, we can express the 4 unknowns in terms of the external excitation $\vec{f}^{\,b}_{\alpha}$

$$\vec{u}^{\,b}_{o} = -\left(\mathbf{R}^{d}_{o,o} + \mathbf{K}^{-1}_{o,o}\right)\left[\mathbf{I} + \mathbf{Z}^{b}_{o,o}\left(\mathbf{R}^{d}_{o,o} + \mathbf{K}^{-1}_{o,o}\right)\right]^{-1} \mathbf{H}^{b}_{o,\alpha}\, \vec{f}^{\,b}_{\alpha} \tag{3.75}$$

$$\vec{f}^{\,b}_{o} = \left[\mathbf{I} + \mathbf{Z}^{b}_{o,o}\left(\mathbf{R}^{d}_{o,o} + \mathbf{K}^{-1}_{o,o}\right)\right]^{-1} \mathbf{H}^{b}_{o,\alpha}\, \vec{f}^{\,b}_{\alpha} \tag{3.76}$$

$$\vec{u}^{\,d}_{o} = -\mathbf{R}^{d}_{o,o}\left[\mathbf{I} + \mathbf{Z}^{b}_{o,o}\left(\mathbf{R}^{d}_{o,o} + \mathbf{K}^{-1}_{o,o}\right)\right]^{-1} \mathbf{H}^{b}_{o,\alpha}\, \vec{f}^{\,b}_{\alpha} \tag{3.77}$$

$$\vec{f}^{\,d}_{o} = -\left[\mathbf{I} + \mathbf{Z}^{b}_{o,o}\left(\mathbf{R}^{d}_{o,o} + \mathbf{K}^{-1}_{o,o}\right)\right]^{-1} \mathbf{H}^{b}_{o,\alpha}\, \vec{f}^{\,b}_{\alpha} \tag{3.78}$$

Recall that, equations (3.51) and (3.52) express the blade vibration in terms of the external excitation and the blade base motion. Therefore, the vibrations of the blades can be easily derived by substituting equation (3.75) into equations (3.51) and (3.52).

It is important to notice that the most computationally intensive part in equations (3.75) is to calculate the inverse of the matrix $\left[\mathbf{I} + \mathbf{Z}^{b}_{o,o}\left(\mathbf{R}^{d}_{o,o} + \mathbf{K}^{-1}_{o,o}\right)\right]$. The dimension of this matrix is 6•NB by 6•NB which is significantly smaller than the dimension of a general finite element model of a bladed disk. For a typical bladed disk with, for instance, 65 blades, the finite element model could have thousands of degrees of freedom to be solved for; however, the number of the unknown degrees of freedom is only 390 (= 6•65) if we use the reduced order model.

Chapter 4: COMPARISON OF RESULTS

In Chapter 3, we have developed the algorithm for the reduced order modeling to solve for the forced vibration of bladed disks. In this chapter, the algorithm will be tested on a simplified model problem. A code named LMCC (Linear Mistuning Computer Code) has been developed based on the algorithm. The results of LMCC will be compared with the results of the direct finite element approach to examine the validity of the reduced order model.

4.1 Attachment Stiffness and Damping Ratios

Before we implement the proposed algorithm, there are still several parameters of the reduced order model left to be determined. The first is the attachment stiffness matrix $\mathbf{K}_{o,o}$ which simulates the stiffness of the disk-blade attachments (see equation (3.74)). Because of the simplified geometry of our test problem, the attachment stiffness is effectively infinite. Equation (3.74) then implies the continuity in displacements

$$\vec{u}^{\,d}_{o} = \vec{u}^{\,b}_{o} \tag{4.1}$$

and equations (3.75), (3.76), (3.77), and (3.78) become

$$\vec{u}^{\,b}_{o} = -\mathbf{R}^{d}_{o,o}\left[\mathbf{I} + \mathbf{Z}^{b}_{o,o}\mathbf{R}^{d}_{o,o}\right]^{-1}\mathbf{H}^{b}_{o,\alpha}\vec{f}^{\,b}_{\alpha} \tag{4.2}$$

$$\vec{f}^{\,b}_{o} = \left[\mathbf{I} + \mathbf{Z}^{b}_{o,o}\mathbf{R}^{d}_{o,o}\right]^{-1}\mathbf{H}^{b}_{o,\alpha}\vec{f}^{\,b}_{\alpha} \tag{4.3}$$

$$\vec{u}^{\,d}_{o} = -\mathbf{R}^{d}_{o,o}\left[\mathbf{I} + \mathbf{Z}^{b}_{o,o}\mathbf{R}^{d}_{o,o}\right]^{-1}\mathbf{H}^{b}_{o,\alpha}\vec{f}^{\,b}_{\alpha} \tag{4.4}$$

$$\vec{f}^{\,d}_{o} = -\left[\mathbf{I} + \mathbf{Z}^{b}_{o,o}\mathbf{R}^{d}_{o,o}\right]^{-1}\mathbf{H}^{b}_{o,\alpha}\vec{f}^{\,b}_{\alpha} \tag{4.5}$$

The other parameters of the reduced order model to be determined are the damping ratios of the substructures' modes. Since the mechanism of the structural damping is not well-realized so far, it is difficult to accurately determine these damping ratios by analytical methods. However, since the peak amplitude of a slightly damped system is proportional to the reciprocal of its damping ratios, we are able to determine these damping ratios by numerical experiments. The procedure was used is the following:

1. Assume the damping ratios of the substructures' modes are equal to some small value. A better choice is the damping ratios of the system modes (if they are available) because, based on our experience, the damping ratios of the substructures' modes are in general approximately equal to those of the system modes.

2. Adjust the damping ratios of the substructures' modes such that the peak amplitude of the tuned response of the reduced order model matches that of a reliable source, for example, the physical experiment.

In the following section, we will proceed to design a test problem to examine the validity of the reduced order model.

4.2 Design of the Test Problem

When designing an appropriate test problem, it is necessary to consider the following issues:

1. The test case should represent a realistic object which can vibrate in three-dimensional space. Spring-mass models should be avoided because they are in general unrealistic. Models with beam-type blades will not be considered as appropriate choices either since we intend to check the appropriateness of the rigid blade base assumption; in other words, we want to design a test problem having multiple nodes at each disk-blade interface.

2. The test problem should be simple in geometry so that we can readily check the results based on our physical intuition.

3. The whole system should not have too many degrees of freedom so that it can be analyzed by the finite element method without costing too much computational time or generating the numerical stability problem with the finite element solution.

After considering these requirements, a simplified bladed disk with twenty four blades (Figure 4.1) was chosen to serve our purpose. The finite element model is constructed by using plate bending elements with three degrees of freedom per node, namely, one translation perpendicular to the plane and two rotations parallel to the plane. The thickness of the disk is 0.8 inch and that of the blades is 0.15 inch. The geometry is chosen so that the disk and the nominal blade have the natural frequencies that a typical turbo-pump stage would have. Both the blades and disk were assumed to have material properties associated with a super Nickel alloy.

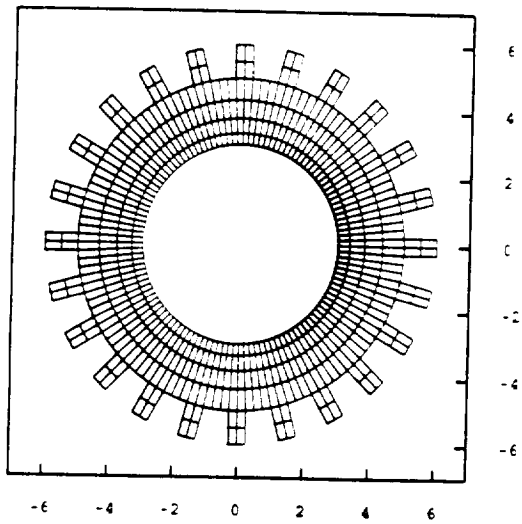

Figure 4-1: Geometry of the test problem (scales are in inches). Thickness of the disk: 0.80 in. Thickness of the blades: 0.15 in.

4.3 Tuned System Responses*

4.3.1 Resonant frequencies and mode shapes

From [7], we know that, if the blades are perfectly tuned, the j-th engine order traveling excitation can excite only a certain family of modes. This family of modes has the characteristics that the phase difference between the neighboring substructures is $j\Delta\varphi$, where N is the number of blades and

$$\Delta\varphi = \frac{2\pi}{N} \tag{4.6}$$

Based on the above knowledge, we can find the resonant frequencies for every family of system modes associated with a specific integer j by finding the forced response peaks of the bladed disk that result from the j-th engine order excitation.

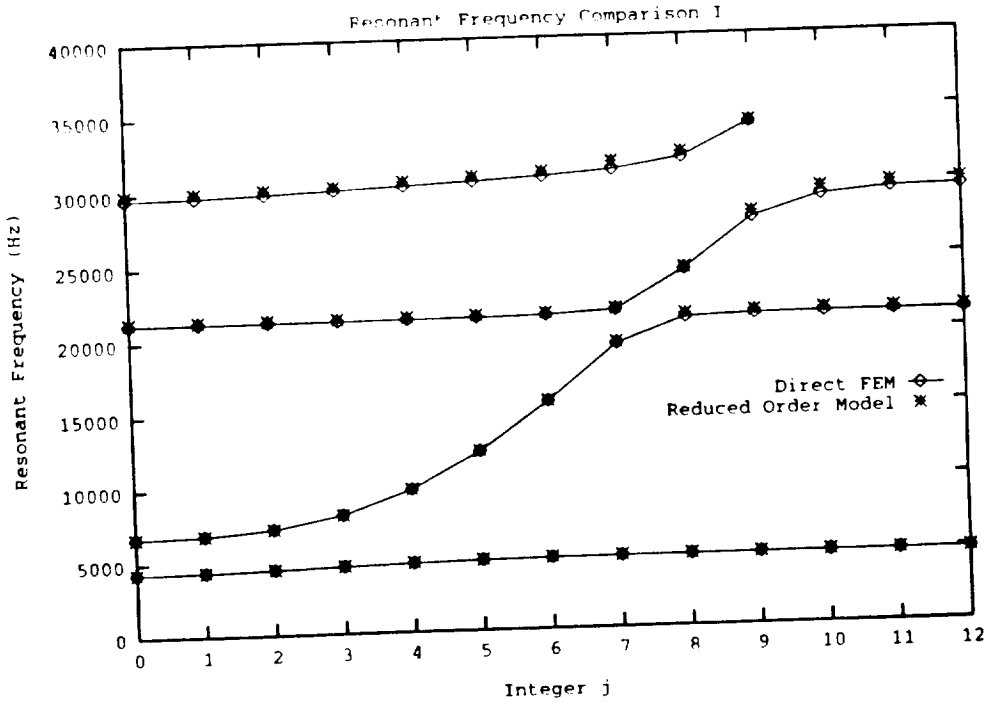

Figure 4-2: Resonant frequencies for the tuned bladed disk predicted by direct FEM and reduced order model

Figure 4.2 shows the resonant frequencies of the tuned bladed disk predicted by two different techniques. The horizontal axis is the integer j mentioned above and the vertical axis

* The reduced order model used in this section has infinitely large attachment stiffness for disk-blade interfaces and experimentally decided damping parameters as discussed in Section 4.1.

is the resonant frequency predicted. The first technique, whose results are depicted by diamonds, is the direct finite element approach. Using this method, we first find the modes of the entire bladed disk, and, secondly, use the standard Mode Superposition Method to calculate the forced responses of the system. The second technique, whose results are depicted by stars, is the reduced order approach. It is apparent that there is reasonably good agreement between the frequency predictions of these two approaches. It is also apparent that LMCC predicts slightly higher frequencies, probably because the assumption of rigid body motion at blades' bases slightly over-constrained the system.

It is worth noticing that the resonant frequencies of the system follow the blade alone frequencies and disk alone frequencies in a particular pattern (Figure 4.3). The blade alone frequencies, which are depicted by the horizontal dashed lines in Figure 4.3 are the natural frequency for a blade rigidly constrained at its base. For this particular blade model, the first blade alone frequency, 4893 Hz, is associated with the first easewise bending mode, the second blade alone frequency, 21387 Hz, is associated with the first torsional mode, and the third blade alone frequency, 30559 Hz, is the second easewise bending mode. There exists no stiffwise bending modes because the type of finite elements we chose does not have degrees of freedom in the stiffwise direction. The disk alone frequencies, which are depicted by squares, are the natural frequencies of the disk with a clamped inner edge and a free outer edge.

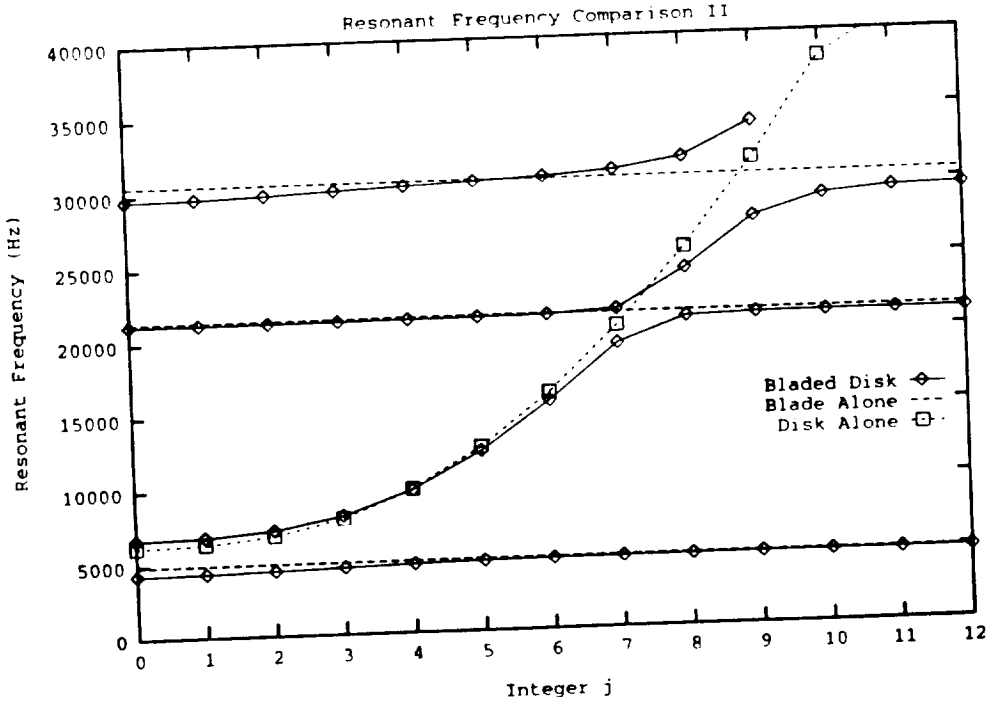

Figure 4-3: Relation between the system frequencies and the natural frequencies of the substructures

Let us now classify the system modes into four groups as indicated by the four solid lines in Figure 4.3 and number these groups from the bottom to the top of the figure. It is observed that the group-1 system frequencies follow the natural frequency of the first blade-alone bending mode very closely. When the system frequency is close to the blade alone frequency and far away from the disk alone frequency, the corresponding system mode has the tendency that the disk remains still and the blades vibrate in the associated blade alone mode. Examples of this kind of "blade-type" system modes derived from the finite element analysis are shown in Figure 4.4 and 4.5. Figure 4.4 shows a system mode with the phase difference between blades being 4 $\Delta\varphi$. For this particular mode, the blades vibrate predominantly in their first bending mode and the disk hardly participates in the vibration though it does have a four-nodal-diameter pattern. Figure 4.5 shows a system mode with the same phase difference between blades. For this particular mode, the blades vibrate predominantly in their first torsional mode and the disk hardly participates.

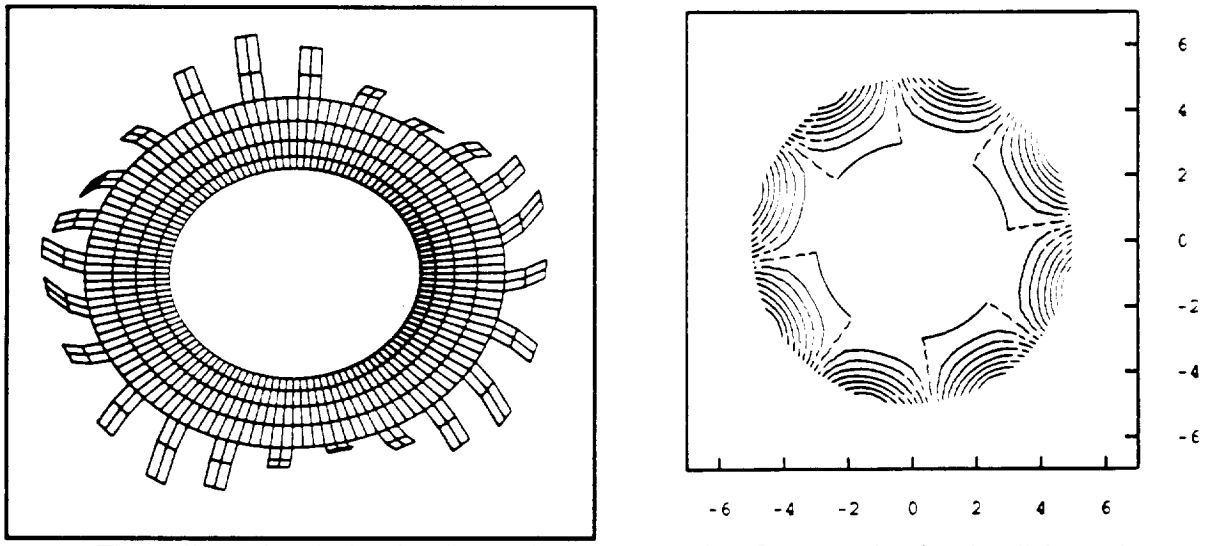

a) Three-dimensional plot for the mode shape

b) Contour plot for the disk portion

Figure 4-4: Mode #9 of the bladed disk (natural frequency = 4682.3 Hz). For this particular mode, the disk hardly participates in the vibration. The integer j = 4.

The group-2 system frequencies follow the disk alone frequencies initially (from j=1 to j=6) and then follow the natural frequency of the first blade-alone torsional mode (from j=8 to j=12). When the system frequency is far away from the blade alone frequency but close to the disk alone frequency, the corresponding system mode has the tendency that the disk vibrates in the associated disk alone mode and the blades follow the disk without much deformation. Figure 4.6 shows an example of this kind of "disk-type" system mode derived

from finite element analysis where the phase difference between blades are 4 $\Delta\varphi$. For this particular mode, the blades follow the disk's vibration passively while the four-nodal-diameter disk modes vibrate vigorously. The last few system modes in group 2 (from j=8 to j=12) are the modes where the disk tends to remain still and the blades tend to vibrate predominantly in their first torsional mode.

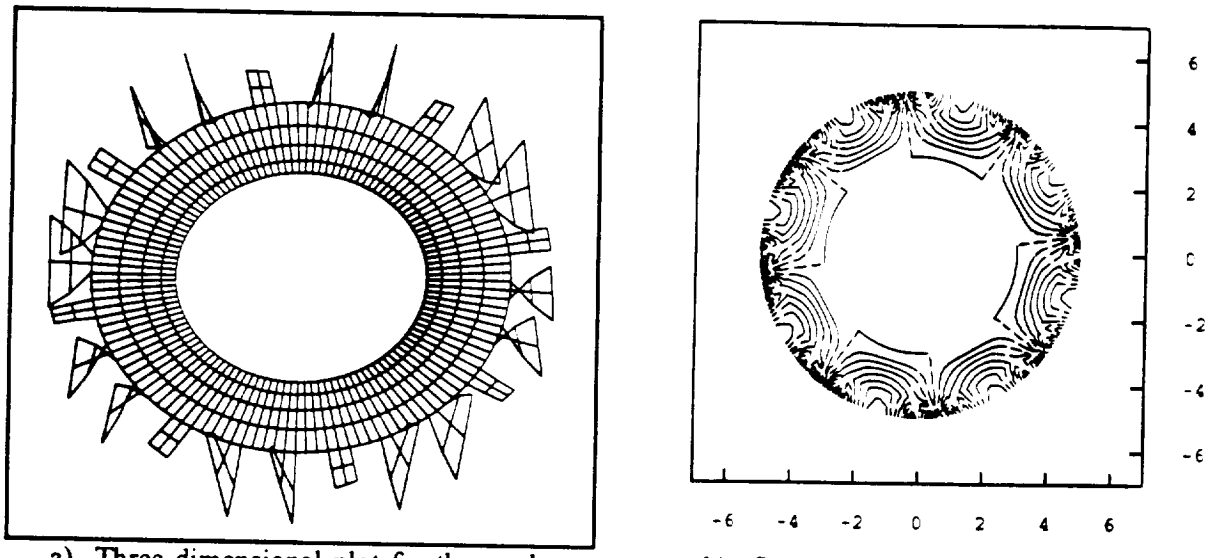

a) Three-dimensional plot for the mode shape

b) Contour plot for the disk portion

Figure 4-5: Mode #57 of the bladed disk (natural frequency = 21260 Hz). For this particular mode, the disk hardly participates in the vibration. The integer j = 4.

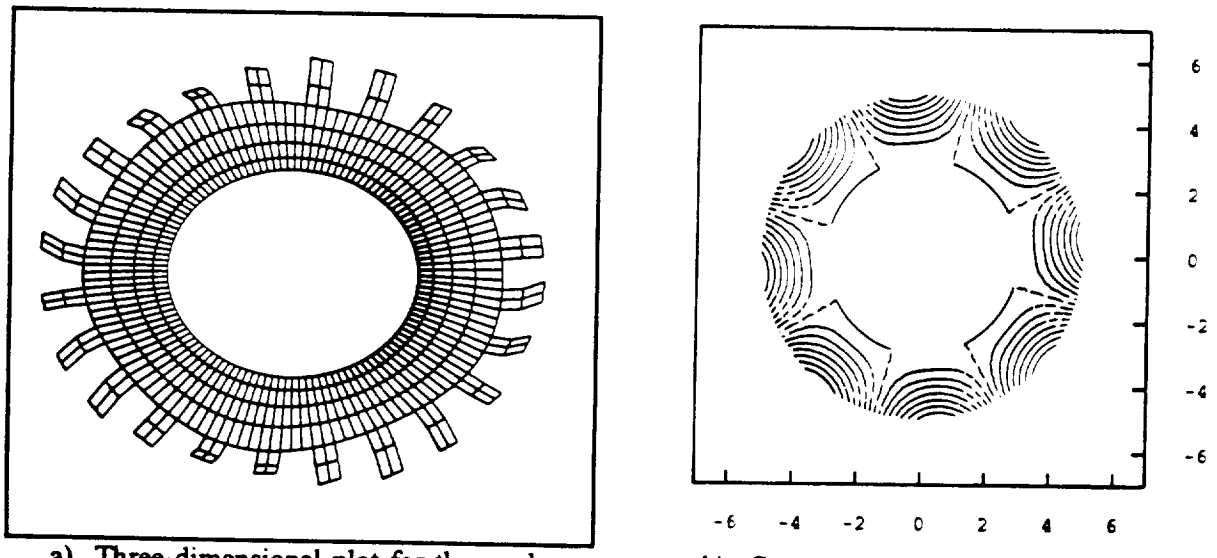

a) Three-dimensional plot for the mode shape

b) Contour plot for the disk portion

Figure 4-6: Mode #33 of the bladed disk (natural frequency = 9714.5 Hz). For this particular mode, the disk strongly participates in the vibration. The integer j = 4.

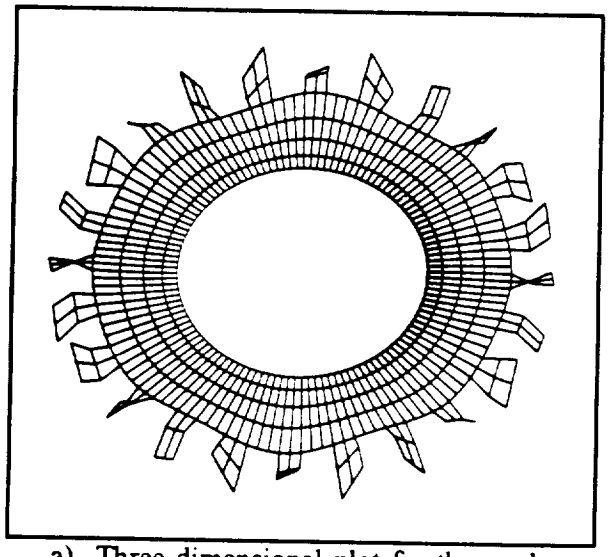

a) Three-dimensional plot for the mode shape

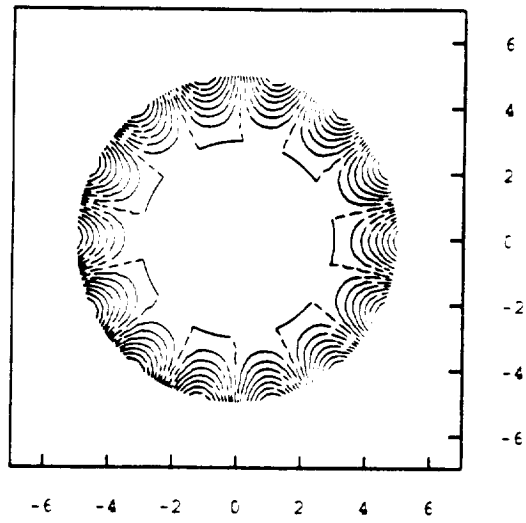

b) Contour plot for the disk portion

Figure 4-7: Mode #39 of the bladed disk (natural frequency = 19265 Hz). This is a mixed-type mode. The integer j = 7.

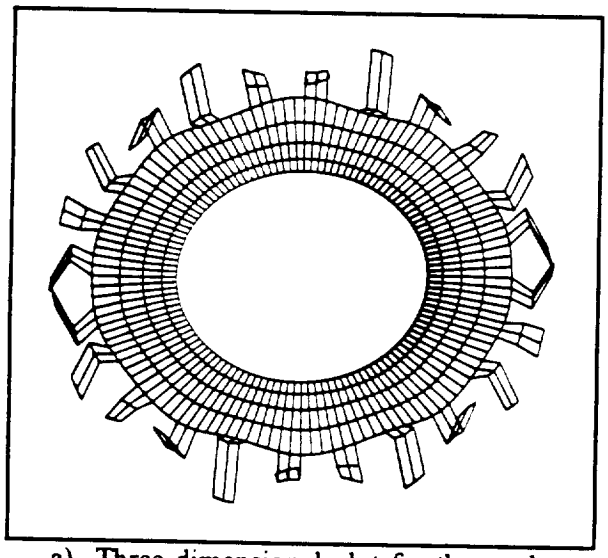

a) Three-dimensional plot for the mode shape

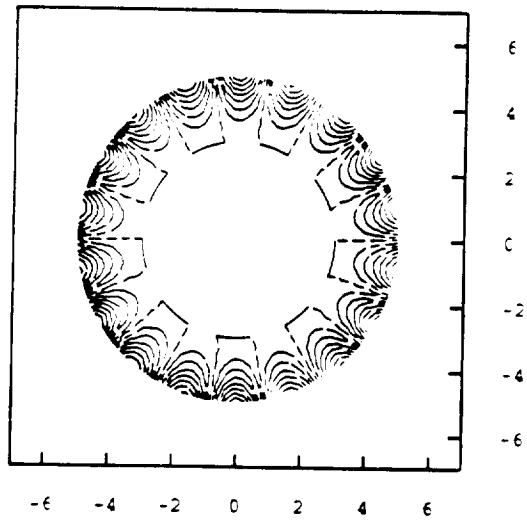

b) Contour plot for the disk portion

Figure 4-8: Mode #67 of the bladed disk (natural frequency = 27593 Hz). This is a mixed-type mode. The integer j = 9.

In addition to the blade-type and disk-type system modes, there are also the "mixed-type" system modes. System modes of this type often have natural frequencies close to or far from both blade alone frequencies and disk alone frequencies. They are in transition between blade-type and disk-type behavior. Examples of the mixed-type system modes are

shown in Figure 4.7, for a group-2 system mode with 7 $\Delta\varphi$ phase difference between blades, and in Figure 4.8, for a group-3 system mode with 9 $\Delta\varphi$ phase difference between blades.

4.3.2 Tuned response curves

After confirming that the reduced order model works reasonably well in predicting the system frequencies, we would like to see if the response curves predicted by the reduced order model agree well with those predicted by the direct finite element approach. For the purpose of comparison, we will also present the result predicted by BLDVIB [8]. BLDVIB is a numerical code for the vibration analysis of bladed disks. It uses a spring-mass model to represent the bladed disk.

Figure 4.9 (a), (b), and (c) are the tuned response curves of the blade tips predicted by the three different methods. In this particular case, the bladed disk is subjected to a fourth engine order excitation and the participating system modes are the blade-type modes with blades in bending. It appears that the three curves agree well with each other though the response predicted by the reduced order model shifts to a slightly higher frequency. Figure 4.10 depicts similar plots for a blade-type mode with blades in torsion. It is observed again that responses predicted by both LMCC and BLDVIB agree with the response predicted by the direct finite element approach.

4.4 Mistuned System Responses*

In this section, we will compare the mistuned response of the bladed disk predicted by the three approaches mentioned in the previous section. The bladed disk is mistuned in the sense that there are frequency variations from blade to blade. To ensure that the three approaches solve for the response of the same mistuned bladed disk, we modified the code of BLDVIB so that it can read the mistuned blade alone frequencies from the same source that LMCC does. For the direct finite element approach, we simulate the blade frequency variations by changing the Young's modulus of each blade. Typical response curves for the blade-type, disk-type, and the mixed-type vibrations will be examined.

* The reduced order model used in this section has infinitely large attachment stiffness for disk-blade interfaces and experimentally decided damping parameters as discussed in Section 4.1.

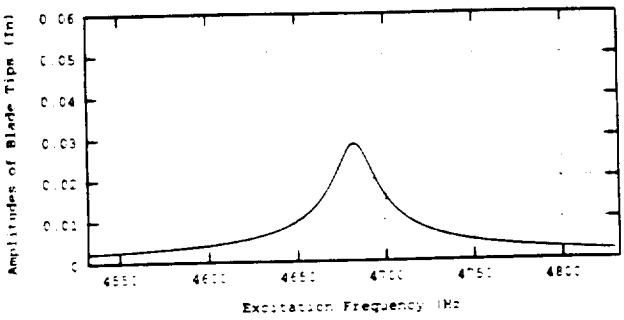

a. Direct FEM

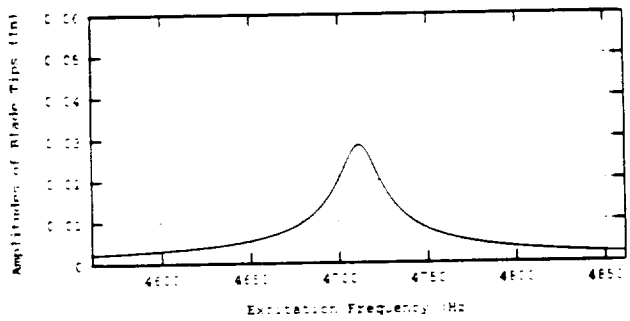

b. LMCC

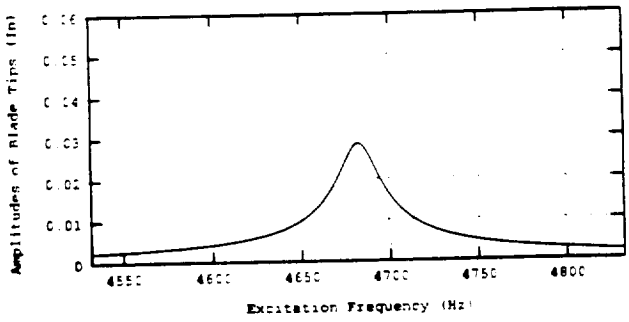

c. BLDVIB

Figure 9: Tuned response curves using three different approaches. System is subjected to a fourth engine order excitation. Blades predominantly vibrate in a first bending mode.

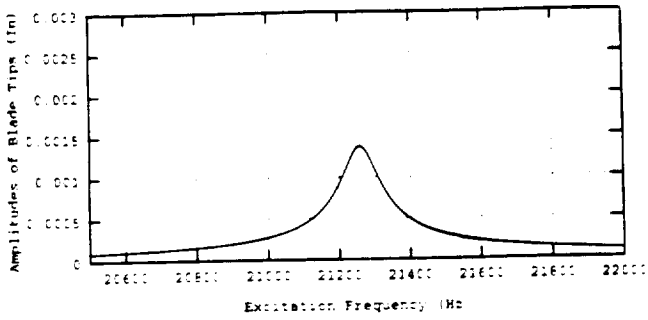

a. Direct FEM

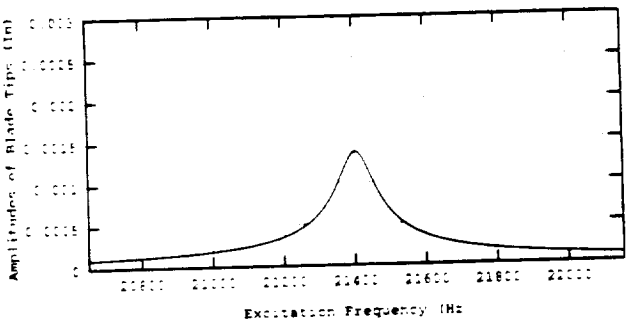

b. LMCC

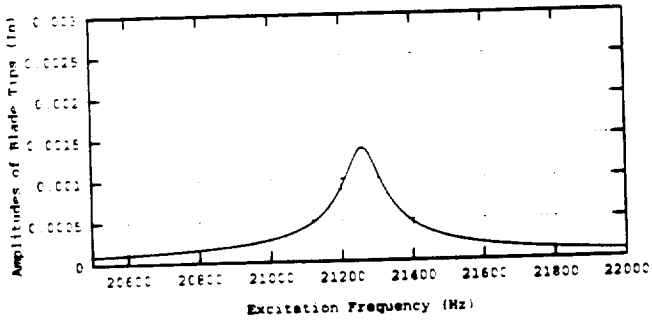

c. BLDVIB

Figure 10: Tuned response curves using three different approaches. System is subjected to a fourth engine order excitation. Blades predominantly vibrate in a first torsional mode.

4.4.1 Blade-type system vibration

Figure 4.11 (a), (b), and (c) are the typical mistuned response curves of the blade tips predicted by the three different approaches. In this case, the bladed disk is subjected to a fourth engine order excitation and the participating system modes are basically the blade-type modes with blades in bending. The tuned response induced by the same excitation was discussed in the previous section (Figure 4.9). It appears that the reduced order model and the spring-mass model give equally good results.

Figure 4.12 shows the mistuned response curves of the blade tips predicted by the three different approaches. In this case, the bladed disk is subjected to a fourth engine order excitation and the participating system modes are the blade-type modes with blades in torsion. The response of the tuned stage was discussed in the previous section (Figure 4.10). We can see that LMCC works much better than BLDVIB, though they predict equally well the results for the tuned stage. One of the possible explanation for the failure of BLDVIB in this particular case is that the spring-mass model does not account for the effects of three-dimensional motion and multiple node attachment at the disk-blade interfaces. By observing Figure 4.12(c), we also find that the blades do not interact as much as they should. This leads to another possible reason for the failure of the spring-mass model that they can not account for the complicated blade-to-blade coupling effect while the blades vibrate predominantly in their first torsional mode.

4.4.2 Disk-type system vibration

Figure 4.13 shows the comparison of the mistuned results predicted by the direct finite element approach and the reduced order model. For this particular case, the bladed disk is subjected to a fourth engine order excitation and the disk participates vigorously in the vibration since the natural frequency of the four-nodal-diameter disk modes is very close to the system frequency. It appears the result predicted by the reduced order model agrees well with the result predicted by the direct finite element approach. It is interesting to observe that the blade mistuning does not affect the disk-type vibration very much.

4.4.3 Mixed-type system vibration

Figure 4.14 and Figure 4.15 are the mistuned responses for the mixed-type system vibration. The vibration is mixed in the sense that both the disk and the blades participate in the vibration and it is hard to tell which blade alone mode the blades vibrate in. Figure 4.14 shows the response curves for the mistuned bladed disk under a seventh engine order excitation. Figure 4.15 shows the response curves for a mistuned bladed disk under a ninth

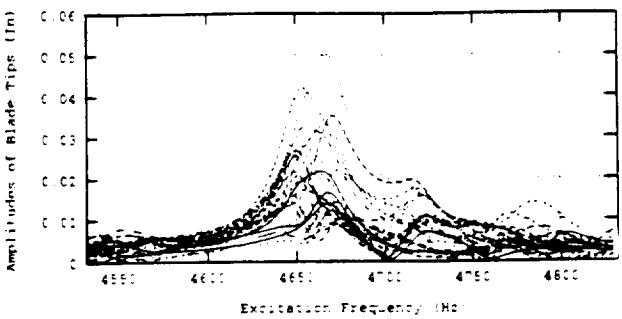

a. Direct FEM

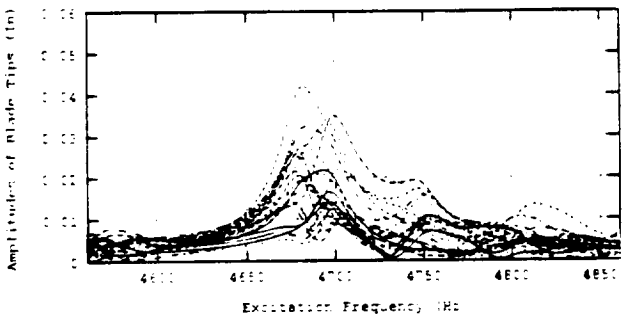

b. LMCC

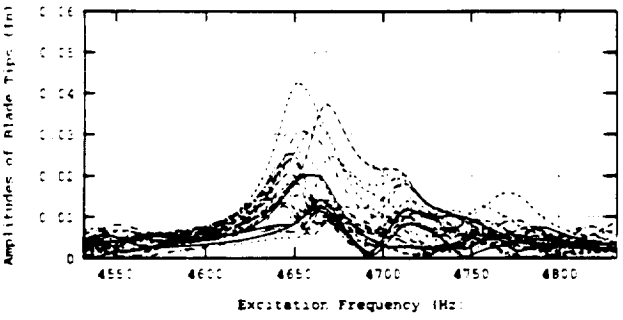

c. BLDVIB

Figure 11: Mistuned response curves predicted by three different approaches. System is subjected to a fourth engine order excitation. Blades predominantly vibrate in a first bending mode.

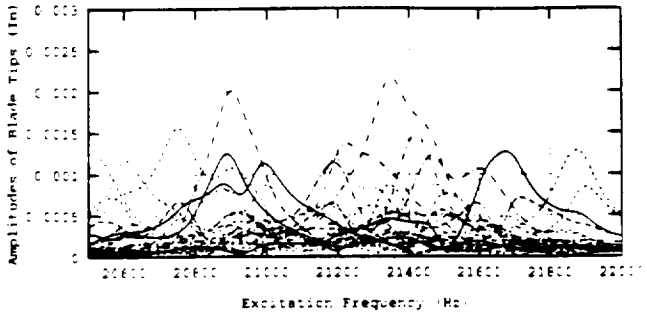

a. Direct FEM

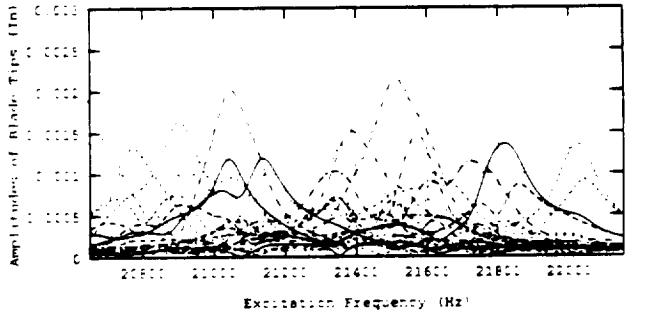

b. LMCC

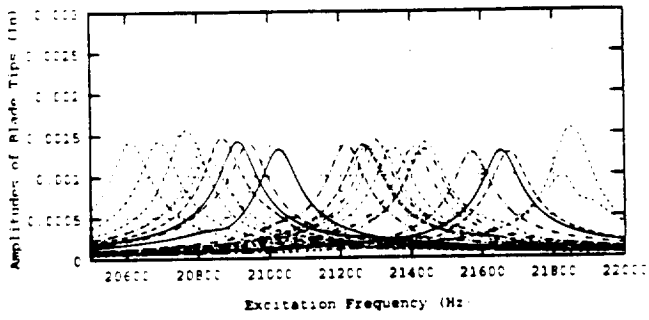

c. BLDVIB

Figure 12: Mistuned response curves predicted by three different approaches. System is subjected to a fourth engine order excitation. Blades predominantly vibrate in a first torsional mode.

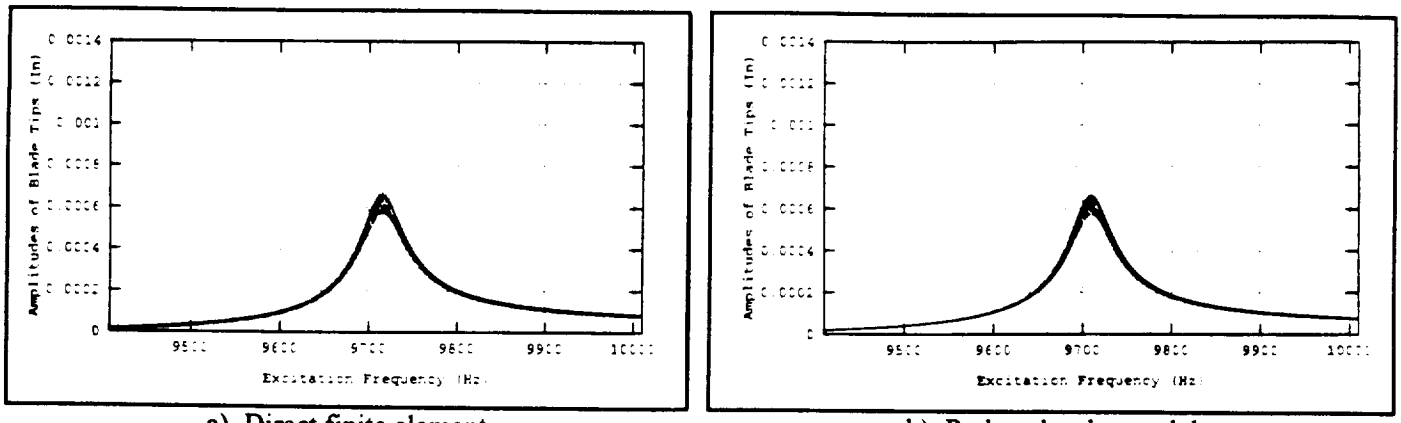

a) Direct finite element b) Reduced order model

Figure 4-13: Mistuned response curves predicted by different approaches. System is subjected to a fourth engine order excitation. The disk strongly participates in the vibration.

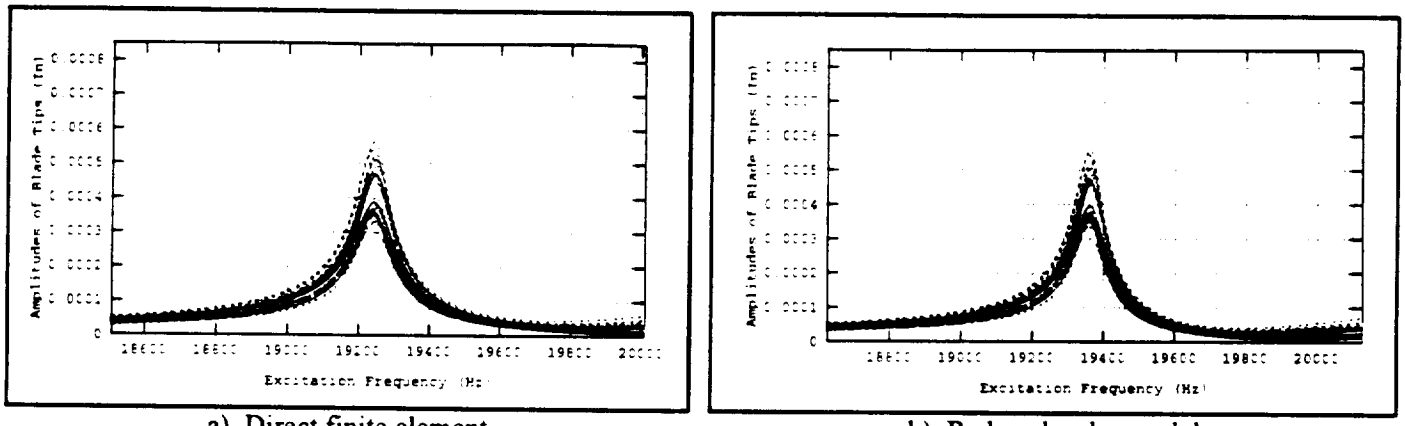

a) Direct finite element b) Reduced order model

Figure 4-14: Mistuned response curves predicted by different approaches. System is subjected to a seventh engine order excitation. Both the disk and blades participate in the vibration.

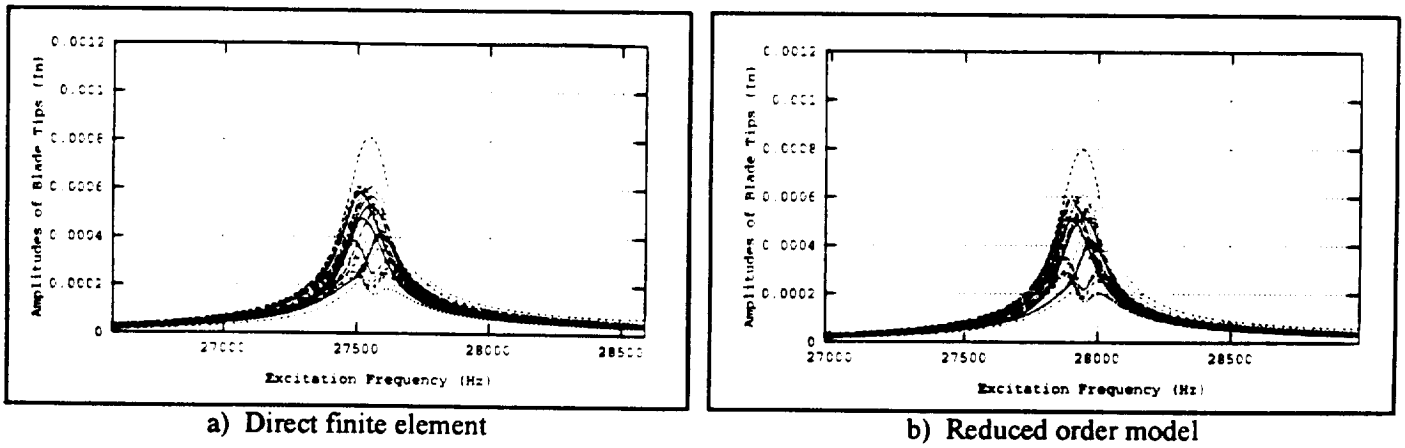

a) Direct finite element b) Reduced order model

Figure 4-15: Mistuned response curves predicted by different approaches. System is subjected to a ninth engine order excitation. Both the disk and blades participate in the vibration.

engine order excitation. It is apparent that the curves predicted by the reduced order model agree very well with the curves predicted by the direct finite element approach.

In the last two sections, we observed that the reduced order model can accurately predict the response of both tuned and mistuned bladed disks. The spring-mass model used by BLDVIB failed to model the coupling effect between blades while the blades vibrate predominantly in their first torsional mode. In the next section we will compare the execution time taken by the direct finite element approach and the reduced order approach.

4.5 Execution Time Comparison

Figure 4.16 shows the execution time comparison between the direct finite element approach and the reduced order approach when using a supercomputer.

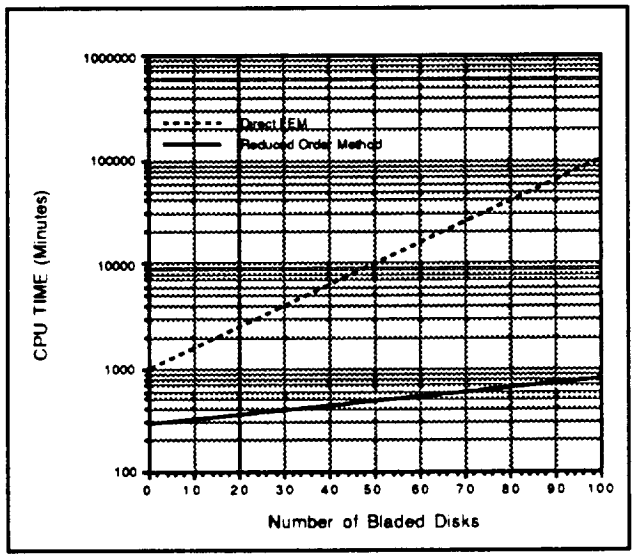

Figure 4.16: Execution time comparison between the direct finite element approach and the reduced order approach.

The data are calculated based on the estimation for a typical bladed disk as following:

Number of blades	50
Number of degrees of freedom of a blade	15,000
Number of degrees of freedom of a disk sector	10,000
Number of degrees of freedom of a bladed disk	1,250,000

The estimated CPU time for solving for 100 system modes is 1,000 CPU minutes per bladed disk. The time for calculating the forced response using Mode Superposition Methods is approximate 0.02 minute for every 100 excitation frequencies. Therefore, we can write down the following equation for the relation between the execution time needed by using the direct finite element approach and the number of bladed disks analyzed,

$$T^{fem} = 1000.02\ N \tag{4.7}$$

where N is the number of bladed disks.

If we use the reduced order approach for the blade mistuning problem, the CPU time for solving for the modes of a nominal blade is approximate 15 minutes and that for the disk modes is approximate 250 minutes provided that the cyclic symmetric boundary conditions are used to improve the computational efficiency. The CPU time needed to process the output of the finite element analysis for the use of LMCC is approximate 15 minutes. And, for every 100 excitation frequencies, LMCC will take approximate 5 minutes to calculate the forced response. Therefore, we can write down the equation for the relation between the execution time needed by using the reduced order approach and the number of bladed disks analyzed,

$$T^{lmcc} = 280 + 5\ N \tag{4.8}$$

An immediate comparison we can obtain from observing equations (4.7) and (4.8) is that, for every additional bladed disk, the direct finite element approach needs 1000 more minutes but LMCC (the reduced order approach) needs only 5 more minutes. Figure 4.16 shows that, for a typical mistuning analysis with 100 bladed disks analyzed, the direct finite element approach needs 100,002 minutes and the reduced order approach needs only 780 minutes.

Chapter 5: CONCLUSIONS AND SUGGESTIONS

5.1 Conclusions

Mistuned vibration of bladed disks has drawn much attention since it can result in large blade-to-blade amplitude variations and the high response blades can fail from high cycle

fatigue. Due to the severe operating conditions that modern aircraft are subjected to, accurate predictions of the vibration of mistuned bladed disks become necessary. Using finite elements to model a bladed disk is not a feasible approach for a thorough mistuning analysis since the geometry of a bladed disk is so complex that a structurally accurate finite element model would have too many degrees of freedom. Using spring-mass models to represent a bladed disk results in low degree-of-freedom formulations. Though they can be efficiently and reliably solved by computers, the ad hoc way in which they choose system parameters and their questionable accuracy are undesirable.

To develop a structurally accurate and computationally efficient model for the bladed disks, we first considered the receptance method. Though the receptance method can significantly reduce the number of degrees of freedom of the system, the resultant equations can still have too many degrees of freedom since the disk and the blade usually contact at multiple points. Its necessity of using free-free blade modes is especially undesirable since, in general, blades tend to vibrate like clamped-free modes and much of the work done on the blades utilizes cantilever blades.

The reduced order modeling follows the idea of the receptance method but further assumes that the blade bases undergo rigid body motion. The blade vibration is considered as a combination of blade base motion and cantilever blade modes. By finding the six equivalent degrees of freedom for the disk vibration at each disk-blade interface, we are able to reduce the number of degrees of freedom of the whole structure down to six times the number of blades. With this significant reduction in the number of unknowns, the reduced order model results in a formulation that can be efficiently solved by computers. Along with its low computational cost, the reduced order model is structurally accurate and provides a straight forward approach for modeling the system since it directly takes the results from the finite element analysis of a tuned system without ad hoc assumptions.

The validity of the reduced order model was examined by applying its algorithm to solve for the forced response of a carefully designed test problem. The test problem is designed so that it represents a realistic object that vibrates in three-dimensional space and has multiple nodes at each disk-blade interface. For the purpose of comparing the reduced order model with other reliable techniques, the geometry of the test problem is relatively simple so that it can be efficiently solved by the direct finite element approach. It is shown in Chapter 4 that the reduced order model can predict the tuned system frequencies reasonably well. By comparing the results from the different approaches, it appears that the reduced order model

is able to capture the characteristics of the mistuned bladed disk. It predicted response curves that are almost identical to the results of the direct finite element approach for the more than one hundred cases examined, of which the cases presented in Chapter 4 were representative. The results predicted by a typical spring-mass model are also examined. It appears that the spring-mass model predicts mistuned responses well when the blades vibrate in bending modes but predicts poorly when the blades vibrate in high frequency torsional modes.

Based on the investigations we have done, we can conclude that the reduced order model is a valuable model for the vibration analysis of mistuned bladed disks. It is valuable for the following reasons:

1. It is structurally accurate and can be used for bladed disks of various kinds of geometry because it utilizes the output of general finite element models instead of being restricted to springs and masses or plates and beams.

2. It is straight forward in the sense of modeling since the system parameters are directly taken from the output of the finite element analysis instead of making ad hoc assumptions.

3. It is computationally efficient because the number of degrees of freedom of its formulation is only six times the number of blades. This number is significantly smaller than that of a finite element model and of the same order of that of a more complicated spring-mass model, for example, [9].

5.2 Suggestions

One of the subjects of bladed disk vibration under intensive study nowadays is the friction related mistuning problem. Blade-to-blade and blade-to-ground friction dampers are integrated into the bladed disk assemblies to dissipate energy so that the peak amplitudes of blade vibration can be reduced. Since the nonlinear friction forces are sensitive to the displacements and, sometimes, to the velocities of the blades, it is necessary for the analysts to have a structurally accurate model. Much of the work has been done on this subject is based on spring-mass models. With proper tuning, spring-mass models often predict reasonably accurate responses for a linear system; however, their ability in predicting the response of a nonlinear system is questionable since friction forces can considerably change the mode shapes of the blades and this change can hardly be modeled by simple spring-mass systems.

It is, therefore, reasonable to use the reduced order model for the analysis of friction related mistuning problems. Because of the computational efficiency of the reduced order model, we can easily derive the receptance for the friction interfaces of the bladed disk. It is then possible to use this structurally accurate receptance to solve for the friction problem either by time integration methods or by approximation techniques.

REFERENCES

[1] El-Bayoumy, L. E. and Srinivasan, A. V., "Influence of Mistuning on Rotor-Blade Vibrations," *AIAA Journal*, vol. 13, no. 4, April, 1975, pp. 460-464.

[2] Fabunmi, J. A., "Forced Vibrations of a Single Stage Axial Compressor Rotor," *Journal of Engineering for Power, Transactions of the ASME*, vol. 102, April, 1980, pp. 322-328.

[3] Wildheim, S. J., "Natural Frequencies of Rotating Bladed Disks Using Clamped-Free Blade Modes," *Journal of Vibration, Acoustics, Stresses, and Reliability in Design, Transactions of the ASME*, vol. 105, October, 1983, pp. 416-424.

[4] Griffin, J. H. and Hoosac, T. M., "Model Development and Statistical Investigation of Turbine Blade Mistuning," *Journal of Vibration, Acoustics, Stresses, and Reliability in Design, Transactions of the ASME*, vol. 106, April, 1984, pp. 204-210.

[5] Ewins, D. J., "Structural Dynamic Characteristics of Bladed Assemblies," *ALGOR Manual on Aeroelasticity in Axial-Flow Turbomachines*, vol. 2, Specialized Printing Service Limited, Loughton, 1988, pp. 15-1 to 15-37.

[6] Bishop, R. E. D. and Johnson, D. C., *Mechanics of Vibration*, Cambridge University Press, 1960.

[7] Wagner, L. F., "Vibration Analysis of Grouped Turbine Blades," , Ph.D. Thesis, Carnegie Mellon University, Pittsburgh, PA, 1993.

[8] Griffin, J. H., "An Improved Method of Measuring Blade Vibration and Predicting Engine Durability," Report No. AFWAL-TR-86-2118, Griffin Consulting, Pittsburgh, PA, 1987.

[9] Muszynska, A. and Jones, D. I. G., "A Parametric Study of Dynamic Response of a Discrete Model of Turbomachinery Bladed Disk," *Journal of Vibration, Acoustics, Stress, and Reliability in Design, Transactions of the ASME*, vol. 105, October 1983, pp. 434-443.

[10] Leissa, A. W., "Vibrational Aspects of Rotating Turbomachinery Blades," *Applied Mechanics Reviews*, vol. 34, no. 5, 1981, pp. 629-635.

[11] Crawleyi, E. F. and Mokadam, D. R., "Stagger Angle Dependence of Inertial and Elastic Coupling in Bladed Disks," *Journal of Vibration, Acoustics, Stress, and Reliability in Design*, vol. 106, April 1984, pp. 181-188.

[12] Rzadkowski, R., "The General Model of Free Vibrations of Mistuned Bladed Discs, Part I: Theory," *Journal of Sound and Vibration*, vol. 173, no. 3, 1994, pp. 377-393.

[13] Rzadkowski, R., "The General Model of Free Vibrations of Mistuned Bladed Discs, Part II: Numerical Results," *Journal of Sound and Vibration*, vol. 173, no. 3, 1994, pp. 395-413.

[14] Mota Soares, C. A., et al., "Finite Element Analysis of Bladed Disks," ASME *Structural Dynamic Aspects of Bladed Disks Assemblies*, released at ASME 1976 Winter Annual Meeting, Dec. 5-10, 1976, New York, pp. 73-91.

[15] Salama, A. M., et al., "Dynamic Analysis of Bladed Disks by Wave Propagation and Matrix Difference Techniques," ASME *Structural Dynamic Aspects of Bladed Disks Assemblies*, released at ASME 1976 Winter Annual Meeting, Dec. 5-10, 1976, New York, pp. 45-56.

[16] Williams, F. W., "An Algorithm for Exact Eigenvalue Calculations for Rotationally Periodic Structures," *International Journal for Numerical Methods in Engineering*, vol. 23, 1985, pp. 609-622.

[17] Cai, C. W., Cheung, Y. K., and Chan, H. C., "Uncoupling of Dynamic Equations for Periodic Structures," *Journal of Sound and Vibration*, vol. 139, no. 2, 1990, pp. 253-263.

[18] Pierre, C. and Murthy, D. V., "Aeroelastic Modal Characteristics of Mistuned Blade Assemblies: Mode Localization and Loss of Eingenstructure," Report No. ICOMP-91-12, NASA Technical Memorandum 104519, July 1991.

[19] Lin, C-C. and Mignolet, M. P., "Effects of Damping and Damping Mistuning on the Forced Vibration Response of Bladed Disks," ASME Report No. 93-GT-194, presented at the International Gas Turbine and Aeroengine Congress and Exposition, Cincinnati, Ohio, May 24-27, 1993.

[20] Ottarsson, G. and Pierre, C., "A Transfer Matrix Approach to Vibration Localization in Mistuned Blade Assemblies," ASME Report No. 93-GT-115, presented at the International Gas Turbine and Aeroengine Congress and Exposition, Cincinnati, Ohio, May 24-27, 1993.

[21] Kaza, K. R. V. and Kielb, R. E., "Flutter of Turbofan Rotors with Mistuned Blades," *AIAA Journal*, vol. 22, no. 11, November 1984.

[22] Davis, P. J., *Circulant Matrices*, John Wiley & Sons, 1979.

NASA-CR-197285

NASA
National Aeronautics and Space Administration

Report Documentation Page

1. Report No.	2. Government Accession No.	3. Recipient's Catalog No.

4. Title and Subtitle

Modeling the Effect of Shroud Contact and Friction Dampers on the Mistuned Response of Turbopumps

Final Report (May 31, 1991 through August 31, 1994)

5. Report Date

6. Performing Organization Code

7. Author(s)

J. H. Griffin
M-T. Yang

8. Performing Organization Report No.

10. Work Unit. No.

9. Performing Organization Name and Address

George C. Marshall Space Flight Center
Marshall Space Flight Center, AL 34812

11. Contract or Grant No.
NAS8-38348

13. Type of Report and Period Covered
Contractor Report (5-14-91 to 8-31-94)

12. Sponsoring Agency Name and Address

National Aeronautics and Space Administration
George C. Marshall Space Flight Center
Washington, DC 20546-0001

14. Sponsoring Agency Code

15. Supplementary Notes

Department of Mechanical Engineering
Carnegie Mellon University
Pittsburgh, PA 15213

OCIT
4/0 91
79P

16. Abstract

The contract has been revised. Under the revised scope of work a reduced order model has been developed that can be used to predict the steady-state response of mistuned bladed disks. The approach has been implemented in a computer code, LMCC. It is concluded that: the reduced order model displays structural fidelty comparable to that of a finite element model of an entire bladed disk system with significantly improved computational efficiency; and, when the disk is stiff, both the finite element model and LMCC predict significantly more amplitude variation than was predicted by earlier models. This second result may have important practical ramifications, especially in the case of integrally bladed disks.

17. Key Words (Suggested by Author(s))	18. Distribution Statement
Blade vibration, resonance, mistuning, friction damping, nonlinear constraints	Unclassified – Unlimited

19. Security Classif. (of this report)	20. Security Classif. (of this page)	21. No. of pages	22. Price
		78	

NASA FORM 1626 OCT 86